

2015

^{230}Th and ^{231}Pa on GEOTRACES GA03, the U.S. GEOTRACES North Atlantic transect, and implications for modern and paleoceanographic chemical fluxes

Christopher T. Hayes

Robert F. Anderson

See next page for additional authors

Creative Commons License

[Creative Commons License](#)

This work is licensed under a [Creative Commons Attribution-Noncommercial-No Derivative Works 4.0 License](#).

Follow this and additional works at: <https://digitalcommons.uri.edu/gsofacpubs>

This is a pre-publication author manuscript of the final, published article.

Citation/Publisher Attribution

Hayes, C. T., Anderson, R. F., Fleisher, M. Q., Huang, K.-F., Robinson, L. F., Lu, Y., Cheng, H.,...Moran, S. B. (2015). ^{230}Th and ^{231}Pa on GEOTRACES GA03, the U.S. GEOTRACES North Atlantic transect, and implications for modern and paleoceanographic chemical fluxes. *Deep Sea Research Part II: Topical Studies in Oceanography*, 116, 29-41. doi: 10.1016/j.dsr2.2014.07.007
Available at: <https://doi.org/10.1016/j.dsr2.2014.07.007>

This Article is brought to you for free and open access by the Graduate School of Oceanography at DigitalCommons@URI. It has been accepted for inclusion in Graduate School of Oceanography Faculty Publications by an authorized administrator of DigitalCommons@URI. For more information, please contact digitalcommons@etal.uri.edu.

Authors

Christopher T. Hayes, Robert F. Anderson, Martin Q. Fleisher, Kuo-Fang Huang, Laura F. Robinson, Yanbin Lu, Hai Cheng, R. Lawrence Edwards, and S. Bradley Moran

1 **²³⁰Th and ²³¹Pa on GEOTRACES GA03, the U.S. GEOTRACES North Atlantic Transect,**
2 **and implications for modern and paleoceanographic chemical fluxes**

3 Christopher T. Hayes^{a,b,*}, Robert F. Anderson^{a,b}, Martin Q. Fleisher^a, Kuo-Fang Huang^{c,2}, Laura
4 F. Robinson^{d,e}, Yanbin Lu^f, Hai Cheng^{f,g}, R. Lawrence Edwards^g, S. Bradley Moran^h

5
6 ^aLamont-Doherty Earth Observatory of Columbia University, Palisades, NY, USA

7 ^bDepartment of Earth & Environmental Sciences, Columbia University, New York, NY, USA

8 ^cDepartment of Geology & Geophysics, Woods Hole Oceanographic Institution, Woods Hole,
9 MA, USA

10 ^dDepartment of Marine Chemistry & Geochemistry, Woods Hole Oceanographic Institution,
11 Woods Hole, MA, USA

12 ^eSchool of Earth Sciences, University of Bristol, Bristol, United Kingdom

13 ^fDepartment of Earth Sciences, University of Minnesota, Minneapolis, MN, USA

14 ^gInstitute of Global Environmental Change, Xi'an Jiaotong University, Xi'an, China

15 ^hGraduate School of Oceanography, University of Rhode Island, Narragansett, RI, USA

16 *corresponding author: tel: +1 (617) 324-0283, fax: +1 (617) 253-8630; Mailing address:
17 Massachusetts Institute of Technology, Department of Earth, Atmospheric and Planetary
18 Sciences, 45 Carleton St., E25-610, Cambridge, MA 02139, USA; Email address:
19 cthayes@mit.edu (C. T. Hayes)

20
21 ¹Present address: Department of Earth, Atmospheric and Planetary Sciences, Massachusetts
22 Institute of Technology, Cambridge, MA, USA

23 ²Present address: Institute of Earth Sciences, Academia Sinica, Taipei, Taiwan

24
25
26 Keywords: GEOTRACES, North Atlantic Ocean, thorium, protactinium, scavenging, ventilation
27

28 **Abstract**

29

30 The long-lived uranium decay products ^{230}Th and ^{231}Pa are widely used as quantitative tracers of
31 adsorption to sinking particles (scavenging) in the ocean by exploiting the principles of
32 radioactive disequilibria. Because of their preservation in the Pleistocene sediment record and
33 through largely untested assumptions about their chemical behavior in the water column, the two
34 radionuclides have also been used as proxies for a variety of chemical fluxes in the past ocean.
35 This includes the vertical flux of particulate matter to the seafloor, the lateral flux of insoluble
36 elements to continental margins (boundary scavenging), and the southward flux of water out of
37 the deep North Atlantic. In a section of unprecedented vertical and zonal resolution, the
38 distributions of ^{230}Th and ^{231}Pa across the North Atlantic shed light on the marine cycling of
39 these radionuclides and further inform their use as tracers of chemical flux. Enhanced scavenging
40 intensities are observed in benthic layers of resuspended sediments on the eastern and western
41 margins and in a hydrothermal plume emanating from the Mid-Atlantic Ridge. Boundary
42 scavenging is clearly expressed in the water column along a transect between Mauritania and
43 Cape Verde which is used to quantify a bias in sediment fluxes calculated using ^{230}Th -
44 normalization and to demonstrate enhanced ^{231}Pa removal from the deep North Atlantic by this
45 mechanism. The influence of deep ocean ventilation that leads to the southward export of ^{231}Pa is
46 apparent. The $^{231}\text{Pa}/^{230}\text{Th}$ ratio, however, predominantly reflects spatial variability in scavenging
47 intensity, complicating its applicability as a proxy for the Atlantic meridional overturning
48 circulation.

49

50 **1. Introduction**

51 The motivations to quantify chemical fluxes in the ocean are manifold. For instance,
52 marine biological productivity is set by the balance between nutrient sources and sinks in surface
53 waters and global climate is influenced by the redistribution of heat and salt associated with the
54 ocean's overturning circulation. The well-known rates of radioactive production and decay of
55 ^{230}Th and ^{231}Pa (half-lives 75.69 kyr (Cheng et al., 2000) and 32.76 kyr (Robert et al., 1969),
56 respectively), in addition to their insoluble nature, make them attractive tools to quantify the
57 rates of the marine processes in which they are involved. These include removal from the water
58 column by adsorption to particles (scavenging, related to biological productivity), redistribution
59 by ocean circulation (related to heat transport), and sedimentation to the seafloor (providing a
60 record of past biological productivity, ocean circulation, and more). Unfortunately, the
61 influences of these processes on radionuclide distributions are potentially convolved. This study
62 aims to utilize the spatial distribution of ^{230}Th and ^{231}Pa across the U.S. GEOTRACES North
63 Atlantic Transect (Fig. 1) to characterize the modern cycling of these isotopes in an effort to
64 more completely calibrate their use as flux tracers in the modern and past ocean.

65 Because their production (^{234}U and ^{235}U decay, respectively) is uniform throughout the
66 ocean (Andersen et al., 2010; Delanghe et al., 2002; Robinson et al., 2004; Weyer et al., 2008),
67 the key question in ^{230}Th and ^{231}Pa cycling in the water column is the balance between removal
68 mechanisms. These are primarily (1) the downward flux by scavenging onto sinking particles
69 and (2) lateral fluxes by advection and eddy diffusion. If lateral fluxes can be neglected, the
70 concentration of the scavenged nuclide is expected to increase linearly with depth, representing
71 an "equilibrium" between adsorption onto, and desorption from, vertically homogeneous sinking

72 particles, a concept known as reversible scavenging (Bacon and Anderson, 1982; Krishnaswami
73 et al., 1976; Nozaki et al., 1981).

74 Deviations from linearity in the radionuclide profiles therefore signal where this vertical
75 equilibrium is perturbed by lateral fluxes or where the scavenging intensity has changed. This is
76 admittedly a simple approach, as relatively linear depth profiles are not inconsistent with some
77 lateral flux by dispersion (Roy-Barman, 2009; Venchiarutti et al., 2008). In a basin-scale view,
78 nonetheless, characterizing anomalies to the predictions of reversible scavenging is our first step
79 in deconvolving the oceanic ^{230}Th and ^{231}Pa cycles. Three such anomalies, boundary scavenging,
80 the effects of recently ventilated deep water, and bottom scavenging, appear in unprecedented
81 detail in our North Atlantic section (Fig. 1). We now provide a context for these findings.

82 *1.1 Boundary scavenging of ^{230}Th and ^{231}Pa*

83 Boundary scavenging (Bacon, 1988; Bacon et al., 1976; Spencer et al., 1981) is the
84 enhanced removal of scavenged-type elements (Bruland and Lohan, 2003) at ocean margins.
85 When lateral gradients in particle flux exist, as between biologically productive ocean margin
86 regions and oligotrophic ocean interior regions, insoluble elements are removed from the water
87 column by scavenging to a greater extent at the margin versus the interior. The resulting gradient
88 in radionuclide concentration produces a dispersive flux toward the margin from the interior.
89 Lateral transport in the water column toward ocean margins is more significant for ^{231}Pa than for
90 ^{230}Th because it is more slowly removed downward by scavenging. The residence time with
91 respect to scavenging of ^{231}Pa is 50-200 yrs while that for ^{230}Th is 10-40 yrs (Henderson and
92 Anderson, 2003). On the basis of the boundary scavenging concept alone, elevated $^{231}\text{Pa}/^{230}\text{Th}$
93 ratios in both the dissolved and particulate phase at ocean margins are expected (Fig. 2). Prior to
94 this study, the lateral gradients in the dissolved $^{231}\text{Pa}/^{230}\text{Th}$ ratio or in dissolved ^{230}Th (^{231}Pa)

95 concentrations, predicted by the boundary scavenging concept, have not been definitively
96 observed in the North Atlantic.

97 Modeling efforts have concluded that in ~70% of the ocean, ^{230}Th is redistributed
98 laterally by no more than 30% of its in situ production in the water column (Henderson et al.,
99 1999), consistent with available observations from sediment traps (Yu et al., 2001). However, on
100 the basis of sedimentary records some authors have argued that water column ^{230}Th
101 redistribution could be much greater than 30% due to boundary scavenging-type mechanisms,
102 specifically along the equator in the Pacific (Broecker, 2008; Lyle et al., 2005; Lyle et al., 2007).
103 This claim derives from a concern regarding ^{230}Th -normalization, a method for calculating
104 sediment accumulation rates on the basis of sedimentary ^{230}Th concentrations (Bacon, 1984;
105 François et al., 2004). This method assumes that the burial flux of ^{230}Th is equal to its rate of
106 production by ^{234}U decay in the overlying water column, which allows one to correct for the
107 lateral redistribution of sediments at the seafloor (sediment focusing). Because glacial-
108 interglacial changes in sediment focusing have enhanced or diminished apparent accumulation
109 rates by more than a factor of 2 (François et al., 1990; Suman and Bacon, 1989), the approach
110 has been defended on the basis that neglecting a relatively small bias in the assumption that ^{230}Th
111 burial is equivalent to its production in the overlying water column is justified (François et al.,
112 2007; Siddall et al., 2008). One aim of this study is to quantitatively estimate the magnitude of
113 ^{230}Th redistribution due to boundary scavenging.

114 While the effect of boundary scavenging of ^{231}Pa is well-expressed in the Pacific
115 (Anderson et al., 1983; Anderson et al., 1990; Walter et al., 1999; Yang et al., 1986), it is
116 considered to be suppressed in the Atlantic. This is because this basin is ventilated by southward
117 flowing North Atlantic Deep Water (NADW) on timescales (<100-200 yrs) (Broecker et al.,

118 1991) shorter than the Pa residence time with respect to scavenging (Walter et al., 1999; Yu et
119 al., 1996; Yu et al., 2001). This means Pa can be transported south by deep water flow before it
120 can be dispersed to North Atlantic margins. Although some studies have found evidence, in the
121 form of sedimentary $^{231}\text{Pa}/^{230}\text{Th}$ activity ratios above that produced in seawater by uranium
122 decay of 0.093, for the enhanced removal of ^{231}Pa in the upwelling area off Northwest Africa
123 (Legeleux et al., 1995; Lippold et al., 2012b; Mangini and Diester-Haas, 1983), studies of the
124 North American (Anderson et al., 1994; Lippold et al., 2012a) and the northern Brazil (Lippold
125 et al., 2011) margins do not support boundary scavenging of Pa. The dissolved $^{231}\text{Pa}/^{230}\text{Th}$
126 distribution toward the margins of our transect (Fig. 1) will be used to determine the significance
127 of boundary scavenging in the North Atlantic in light of its recent ventilation.

128 *1.2 The impact of Atlantic circulation*

129 The possibility of boundary scavenging notwithstanding, previous studies have
130 demonstrated that deepwater distributions of ^{230}Th and ^{231}Pa are significantly perturbed by the
131 influence of the recent ventilation of NADW (Luo et al., 2010; Moran et al., 1997; Moran et al.,
132 1995; Moran et al., 2002; Scholten et al., 2001; Vogler et al., 1998). Deep convection at sites of
133 deep water formation results in the injection to depth and propagation along deepwater flow
134 paths of ^{231}Pa and ^{230}Th concentrations which are lower than predicted by reversible scavenging
135 (Moran et al., 1997; Moran et al., 1995; Moran et al., 2002). As the water mass ages, isolated
136 from further perturbations to scavenging equilibrium, dissolved ^{230}Th concentrations increase
137 due to exchange with sinking particles, reaching a steady-state distribution relatively rapidly
138 (determined by the residence time of 10-40 yrs), while ^{231}Pa responds more slowly (residence
139 time of 50-200 yrs) because of the differing scavenging rates of the two elements (Moran et al.,
140 2001; Rutgers v. d. Loeff and Berger, 1993). The longer residence time of ^{231}Pa allows for its

141 southward export with NADW, leaving a ^{231}Pa deficit in deep North Atlantic sediments (Yu et
142 al., 1996). This is the basis for using the sedimentary $^{231}\text{Pa}/^{230}\text{Th}$ ratio as an indicator of the
143 strength of the Atlantic meridional overturning circulation (McManus et al., 2004). The present
144 water column transect is also intended to document the impact of ventilation on ^{231}Pa and the
145 $^{231}\text{Pa}/^{230}\text{Th}$ ratio.

146 In the absence of variations in scavenging intensity, one expects ^{230}Th and ^{231}Pa
147 concentrations and the $^{231}\text{Pa}/^{230}\text{Th}$ ratio to increase with water mass age or time since deep water
148 formation. The strongest response to ageing occurs within 1 to 2 water column residence times
149 after deep water formation. Our section is appropriate to test this prediction because deep water
150 age, or the time since deep-water (as averaged below 2 km) has been isolated from the
151 atmosphere, ranges from <50 yrs in the west to >250 yrs in the east (Broecker et al., 1991). We
152 have extracted an estimate of mean age for our North Atlantic transect from a recent inversion of
153 ventilation tracer observations (^{14}C , CFCs, PO_4^* , temperature and salinity) by Khatiwala et al.
154 (2012). These ventilation ages, which represent the time since a water parcel was last at the
155 surface, taking into account contributions from multiple pathways and source regions, are
156 referred to in the text as mean ages.

157 In addition to consideration of water mass ageing, we put our transect into hydrographic
158 context with the salinity and neutral density (γ_n) section in Fig. 1. The dome of salty subtropical
159 mode water, also known as Eighteen Degree Water, is apparent in the upper 500-800 m and is
160 roughly bound at depth by $\gamma_n = 26.65 \text{ kg m}^{-3}$ (LeBel et al., 2008). The remaining density surfaces
161 in Fig. 1 demarcate the boundaries between the various sources of NADW, which are defined
162 most clearly in the Northwest section between Bermuda and Woods Hole, Mass., known as Line
163 W (Toole et al., 2011). These are, in order of increasing density, Upper and Classic Labrador Sea

164 Water, Iceland-Scotland Overflow Water, and Denmark-Strait Overflow Water, which is
165 underlain by Antarctic Bottom Water (AABW, $\gamma_n > 28.125$). While we name the densest layer of
166 water in the western basin AABW, this water mass, far from its source, must have gone through
167 significant mixing with the overlaying NADW.

168 The deep waters of the Northeastern Atlantic (>3 km depth) are not as clearly defined by
169 the contributions to NADW and are characterized by a relatively homogeneous water mass
170 called Northeast Atlantic Deep Water (NEADW). NEADW is sourced by a mixture of NADW
171 and AABW which enters the Northeast basin largely through the Vema Fracture Zone at 11°N
172 (McCartney et al., 1991), with some contribution from the Romanche Trench near the equator
173 (Broecker et al., 1980; Schlitzer, 1987; Schlitzer et al., 1985). The intermediate water in the
174 southeastern portion of the cruise track intersects the northern extent of the salinity minimum
175 (and silicic acid maximum) originating from Antarctic Intermediate Water (AAIW) (Talley,
176 1999; Tsuchiya, 1989), outlined in Fig. 1. Lastly, the high salinity intrusion of Mediterranean
177 Outflow Water (MOW) at ~1 km depth is well represented on the largely south-north part of the
178 transect approaching Portugal.

179 1.3 Bottom scavenging

180 Deep water ^{231}Pa and ^{230}Th concentrations can also be perturbed by changes in
181 scavenging intensity near the seafloor (bottom scavenging) associated with a change in particle
182 concentration or particle composition. Nepheloid layers (Biscaye and Eittrheim, 1977; McCave,
183 1986), or zones up to hundreds of meters above the seafloor of increased particle concentration
184 caused by the resuspension of sediments, have been known to enhance the scavenging of the
185 shorter-lived ^{234}Th (half-life 24.1 days) in the northwest (Bacon and Rutgers v. d. Loeff, 1989;
186 DeMaster et al., 1991) and northeast (Schmidt, 2006; Turnewitsch et al., 2008; Turnewitsch and

187 Springer, 2001) Atlantic. Previous studies in the North Atlantic have suggested that bottom
188 scavenging could reduce the ^{230}Th concentration in deep water, but since the same effect can be
189 achieved via recent water mass ventilation without invoking a change in scavenging intensity,
190 ventilation was the preferred explanation (Moran et al., 1997; Moran et al., 1995; Vogler et al.,
191 1998). However, recent results from the Pacific, where the ventilation effect is not large enough
192 to produce observed radionuclide depletions in deepwater, have confirmed early observations
193 (Bacon and Anderson, 1982; Nozaki and Nakanishi, 1985) that significant bottom scavenging
194 indeed occurs for ^{230}Th (Hayes et al., 2013; Okubo et al., 2012; Singh et al., 2013) and ^{231}Pa
195 (Hayes et al., 2013). Furthermore, nepheloid layers in the South Atlantic have been found to
196 significantly enhance scavenging of ^{230}Th and ^{231}Pa (Deng et al., 2014).

197 Based on extensive observations in the northwest Atlantic of thick nepheloid layers
198 (Biscaye and Eitrem, 1977; Brewer et al., 1976), our transect is well situated to determine the
199 effect of sediment resuspension on ^{230}Th and ^{231}Pa . In addition to increased particle loading,
200 bottom scavenging may also be affected by a change in particle composition. This section is also
201 well suited to test the hypotheses that ^{230}Th and ^{231}Pa are scavenged especially efficiently by
202 authigenic iron and manganese oxide phases associated with hydrothermal activity at the mid-
203 Atlantic ridge (German et al., 1991; German et al., 1993) or by (oxy)hydroxide coatings of
204 particles formed in regions of organic-rich sediment diagenesis at ocean margins (Anderson et
205 al., 1983; Bacon et al., 1976; Shimmield et al., 1986). To infer likely changes in scavenging
206 intensity in our transect, we utilize the distribution of the particle beam attenuation coefficient,
207 C_p , as measured by transmissometer from CTD casts, which is, to first order, linearly related to
208 particle concentration (Bishop, 1986; Gardner et al., 1985), although the sensitivity of C_p to

209 particle concentration is known to vary with particle size and composition (Baker and Lavelle,
210 1984; Richardson, 1987).

211 **2. Methods**

212 The U.S. Geotraces North Atlantic transect (Fig. 1) consisted of two legs, collectively
213 designated GA03 in the global GEOTRACES survey (geotraces.org). KN199-4 (referred to as
214 GT10) from Lisbon, Portugal to Mindelo, Cape Verde was completed in Oct-Nov 2010. KN204-
215 1 (referred to as GT11) from Woods Hole, Massachusetts to Praia, Cape Verde via St. Georges,
216 Bermuda was completed in Nov-Dec 2011. Radionuclide data were produced by three
217 collaborating laboratories which were intercalibrated (Anderson et al., 2012) to analyze
218 dissolved ($<0.45 \mu\text{m}$) and particulate ($0.45\text{-}51 \mu\text{m}$) ^{232}Th , ^{230}Th , and ^{231}Pa in seawater: the
219 Lamont-Doherty Earth Observatory of Columbia University (L-DEO), the Woods Hole
220 Oceanographic Institution (WHOI) and the University of Minnesota (UMN). Five liter water
221 samples were collected using conventional Niskin bottles, filtered with $0.45 \mu\text{m}$ AcropakTM-500
222 filter capsules, and acidified to $\text{pH} = 1.8$ at sea for storage according GEOTRACES protocols.
223 Particulate samples representing 55-350 L of seawater were collected by McLane Research in
224 situ pumps with a redesigned filter holder (Lam and Morris, 2013) using paired $0.8 \mu\text{m}$ Pall
225 Supor800 polyethersulfone filters (Bishop et al., 2012).

226 Th and Pa isotopes (including the added tracers ^{229}Th and ^{233}Pa) were co-precipitated
227 with Fe (oxy)hydroxide for pre-concentration and purification using acid digestions
228 ($\text{HNO}_3/\text{HF}/\text{HClO}_4$, depending on the laboratory) and ion exchange chromatography. Filter
229 samples were co-precipitated with Fe after complete dissolution ($\text{HNO}_3/\text{HClO}_4/\text{HF}$).
230 Radionuclide concentrations were determined by isotope dilution inductively-coupled plasma
231 mass spectrometry. We converted radionuclide mass concentrations to radioactivity units using

232 the conversion factors, 0.7591 $\mu\text{Bq}/\text{fg}$ ^{230}Th and 1.7476 $\mu\text{Bq}/\text{fg}$ ^{231}Pa . The analytical procedures
233 used at L-DEO, WHOI, and UMN have been fully described by Anderson et al. (2012), Auro et
234 al. (2012), and Shen et al. (Shen et al., 2003; Shen et al., 2002; Shen et al., 2012), respectively.

235 We correct measured dissolved radionuclide concentrations for in-growth due to uranium
236 decay during sample storage (Robinson et al., 2004). In-growth during sample storage from
237 particulate U concentrations is negligible (Anderson, 1982). In order to isolate the signature of
238 scavenging in the dissolved phase we also correct ^{230}Th and ^{231}Pa concentrations for a
239 contribution produced by the partial dissolution of U-containing lithogenic material based on
240 dissolved ^{232}Th as described by Hayes et al. (2013), assuming a crustal $^{238}\text{U}/^{232}\text{Th}$ ratio and
241 congruent dissolution of ^{232}Th , ^{230}Th and ^{231}Pa . Similarly, in the particulate phase we correct
242 measured ^{230}Th and ^{231}Pa for a lithogenic component based on particulate ^{232}Th . All radionuclide
243 concentrations discussed in the text are corrected for lithogenic sources and are denoted as “xs”.
244 For more information on data analysis see the metadata associated with these data online
245 (<http://www.bco-dmo.org/dataset/3847> or <http://www.bodc.ac.uk/geotraces/data/>). Forthcoming
246 studies will present and interpret the distribution of ^{232}Th and particulate radionuclides in their
247 own right. These results are used here only for the interpretation of the dissolved (or total) ^{230}Th
248 and ^{231}Pa distributions.

249 **3. Results and Discussion**

250 *3.1 Sections of dissolved ^{230}Th xs and ^{231}Pa xs*

251 Deviations from linear concentration-depth profiles as predicted by the model of
252 reversible scavenging are immediately apparent in the North Atlantic sections (Fig. 3). Both
253 radionuclides display substantial lateral concentration gradients, some of which are clearly
254 related to recent ventilation. Generally, lower concentrations of both radionuclides are found in

255 the western and northern parts of the transect, coincident with younger mean ages (Fig 3E).
256 Additionally low concentrations of ^{231}Pa xs in shallow water (Fig. 3D) take on a dome structure,
257 coinciding with EDW, and are presumably reflective of the rapid (<10 yrs) ventilation of this
258 subtropical mode water (Jenkins, 1988).

259 Notably unrelated to any change in mean age (Fig. 3E), ^{230}Th xs also has reduced
260 concentrations throughout the water column in the section between Cape Verde and Mauritania
261 (Cape Verde transect, Fig. 3B) coincident with increasing particle concentrations (Fig 3A, 5000-
262 6500 km section distance). The plunging isolines of ^{230}Th xs concentration toward the
263 continental margin on this transect are strong evidence for the process of boundary scavenging
264 occurring. We quantify the lateral transport of ^{230}Th xs and ^{231}Pa xs associated with this
265 boundary scavenging in section 3.2.

266 Both radionuclides show vertical concentration anomalies as well. Concentrations
267 generally increase linearly from the surface to depth but nearly always begin to decrease toward
268 the seafloor. These negative deviations with respect to reversible scavenging generally start
269 higher in the water column for dissolved ^{231}Pa xs (2-3 km depth) than for dissolved ^{230}Th xs (4-5
270 km). This is a pervasive feature in the Atlantic (Luo et al., 2010; Moran et al., 2002; Scholten et
271 al., 2008; Scholten et al., 2001; Vogler et al., 1998) which has been largely attributed to the
272 advection of NADW in previous work.

273 At stations GT-10-01, GT11-04, GT11-06, GT11-08, and GT11-10, however, the
274 dissolved radionuclide depletions can be clearly associated with a large increase in beam
275 attenuation related to higher particle concentration (Fig. 3A) and presumably bottom scavenging.
276 Additionally, the near-bottom waters at GT11-16 (mid-Atlantic ridge) and GT10-09 (African
277 margin) have a more modest increase in C_p , but very large dissolved phase depletions. The near-

278 bottom particles at these two sites showed a clear enrichment in metal oxides (Lam et al., this
279 issue), the former being up to 40% authigenic Fe oxides from a hydrothermal plume at the mid-
280 Atlantic ridge, the latter being enrichment of authigenic Fe and Mn oxides (each 2-3% of the
281 particle mass) related to reducing conditions in the surface sediments created by organic matter
282 diagenesis. It thus seems likely that bottom scavenging due to increased particle abundance
283 and/or unique particulate chemistry is at least as significant as ventilation in regulating the
284 distributions of dissolved ^{230}Th xs and ^{231}Pa xs across the North Atlantic. In section 3.3, we give
285 a few examples of how ventilation and bottom scavenging may be convolved in determining
286 ^{230}Th xs and ^{231}Pa xs distributions. The de-convolution of these effects requires sensitivity testing
287 in 3-dimensional ocean models which is beyond the scope of this study.

288 *3.2 Quantification of boundary scavenging*

289 Enhanced removal of trace elements at ocean margins is supported by advective and
290 diffusive fluxes that arise due to the lateral concentration gradients imposed by lateral gradients
291 in scavenging intensity (Bacon, 1988). To quantify the magnitude of this flux, one can calculate
292 the lateral concentration gradients from concentration profiles. Since radionuclides are
293 exchanged between dissolved and adsorbed forms faster than they are removed to the seafloor
294 (Bacon and Anderson, 1982), for mass continuity, one must consider the total radionuclide
295 concentration (dissolved plus particulate). In Figure 4, we plot particulate and total ^{230}Th xs and
296 ^{231}Pa xs for the stations between Mauritania and GT11-22. Total ^{230}Th xs concentrations (Fig.
297 4C) are consistently lower at stations closer to the African margin, at nearly all depths. The
298 lateral gradient in total ^{231}Pa xs (Fig. 4D), on the other hand, is smaller than can be resolved
299 within our analytical uncertainties. These observations are consistent with the boundary
300 scavenging concept (Fig. 2). At the margin, ^{230}Th concentrations can be depleted with respect to

301 ocean interior concentrations to a greater extent than ^{231}Pa concentrations. This is due to the
 302 longer ocean residence time of ^{231}Pa . Lateral mixing and advection is not fast enough to erase the
 303 margin-interior ^{230}Th concentration gradient imposed by scavenging, whereas a lateral flux
 304 toward the margin is supported for ^{231}Pa . Consequently, both dissolved and particulate
 305 $^{231}\text{Pa}/^{230}\text{Th}$ xs ratios are higher at the margin versus the interior (Fig. 4E-F), as predicted by
 306 Bacon (1988).

307 In one dimension (x, an isopycnal surface, since circulation occurs preferentially along
 308 lines of constant seawater density), for total ^{230}Th xs (Th), the steady-state mass balance is:

$$309 \quad \frac{dTh}{dt} = P - S \frac{dTh_p}{dz} - u \frac{dTh}{dx} + K_H \frac{d^2Th}{dx^2} \quad \text{Eq. 1}$$

310 P is production due to ^{234}U decay. S is the particle sinking rate which, when multiplied by the
 311 vertical gradient of particulate ^{230}Th concentration (second term on right-hand side of Eq. 1),
 312 represents the downward flux by scavenging. The third and fourth terms on the right-hand side of
 313 Eq. 1 represents lateral fluxes due to advection (isopycnal velocity, u, multiplied by the first
 314 isopycnal concentration gradient) and eddy diffusion (isopycnal eddy diffusion coefficient, K_H ,
 315 multiplied by the second isopycnal concentration gradient), respectively.

316 In order to affect the steady-state mass balance, the advective and diffusive terms must occur on
 317 a timescale appropriate to the residence time, τ , of the tracer. The residence times, as defined by
 318 the water column inventory of radionuclide divided by its integrated production in the water
 319 column, between GT10-09 and GT11-22 for ^{230}Th and ^{231}Pa , respectively, are 10-28 yrs and 120-
 320 150 yrs. The corresponding length scales over which lateral eddy diffusivity should be
 321 considered are $\sim 800\text{-}1300$ km for ^{230}Th and $2750\text{-}3080$ km for ^{231}Pa ($\Delta x = \sqrt{2K_H\tau}$,
 322 parameterizing eddy diffusivity as a random walk process), using $K_H = 10^3 \text{ m}^2 \text{ s}^{-1}$, as determined
 323 in the Northeast Atlantic (Ledwell et al., 1998). The advective length scale ($\Delta x = u\tau$) depends
 324 linearly on the current speed and will be >1500 km for both radionuclides if u is greater than a
 325 typical deep current speed of 2 mm/s. However, because east-west velocities cyclically change
 326 direction in this region (Zenk et al., 1991) and their magnitude is difficult to estimate for the
 327 deep ocean, we do not attempt to quantify the advective flux.

328 The isopycnal gradients in ^{230}Th are estimated discretely using the observations from
329 GT10-09, GT10-10, GT10-11 and GT10-12 (Fig. 4C). We do not include GT11-22 in the
330 analysis because it makes the transect larger than the ^{230}Th -mixing length scale (~ 1400 km). The
331 isopycnal ^{231}Pa gradients are smaller than can be resolved within our analytical uncertainty. Th-
332 ^{230}Th concentrations were interpolated onto a common set of isopycnals (Fig. 5A), and because
333 GT10-11 and GT10-12 are nearly indistinguishable we average these two profiles and consider
334 the average profile representative of the region at the mid-point between the two stations.
335 Uncertainties were accounted for and propagated in the calculations by assuming a conservative
336 analytical uncertainty for total ^{230}Th xs of 1.5%. Two isopycnal gradients (Fig. 5B) were
337 calculated by differencing the concentration profiles, between GT10-09 and GT10-10 and
338 between GT10-10 and GT10-11/12, and dividing by the lateral distance between the stations. A
339 positive gradient is defined as lower concentration in the east (leading to lateral fluxes toward
340 Mauritania). Then the second isopycnal gradient (Fig. 5C) was calculated by differencing the
341 two isopycnal gradient profiles and dividing by the distance between the mid-points of the
342 stations used to calculate the first gradient (Fig. 5D).

343 The second isopycnal gradient is variable above $\gamma_n = 27.8$ (1.2 km depth), but below this
344 density surface, in the bulk of the water column, the gradient is consistently positive (down
345 gradient toward Mauritania). By multiplying the $d^2\text{Th}/dx^2$ profile by K_H ($10^3 \text{ m}^2 \text{ s}^{-1}$), and
346 integrating with depth (~ 0 -3 km), we estimate the lateral convergence of ^{230}Th xs to the margin
347 (technically between two boxes, encompassing stations GT10-10/11/12 and GT10-09/10,
348 respectively) as $509 \pm 171 \text{ mBq m}^{-2} \text{ yr}^{-1}$. In 3 km of seawater, ^{230}Th production due to U decay
349 is $1237 \text{ mBq m}^{-2} \text{ yr}^{-1}$ and thus the diffusive flux adds $41 \pm 14\%$ to the water column production
350 in the margin box (and removes the equivalent from production in the open-ocean box). This is

351 consistent with the upper limit for the model-derived redistribution of water column ^{230}Th
352 (Henderson et al., 1999).

353 Th-230 normalized sediment fluxes will therefore be biased (underestimated) by up to
354 30-50% for core sites at highly productive continental margins such as offshore Mauritania. The
355 magnitude of the complementary bias (overestimation) in ^{230}Th -normalized fluxes in the interior
356 ocean is likely to be smaller than 30-50%. This is because the ^{230}Th added to the relatively small
357 zone of high productivity at the margin is drawn from a much larger pool of the subtropical
358 North Atlantic gyre. The subtropical gyre ^{230}Th budget, however, cannot be fully constrained
359 here because there are likely additional lateral removal fluxes of ^{230}Th to other more expansive
360 high productivity regions such as the equatorial or subpolar North Atlantic (Henderson et al.,
361 1999).

362 Interestingly, the degree of boundary scavenging (and its impact on lateral ^{230}Th
363 redistribution) may have changed since the last glacial maximum (Lao et al., 1992). Nonetheless,
364 the 40% redistribution estimate can be seen as close to a global maximum (in the modern ocean
365 at least) since the Canary Current upwelling regime in which our observations are made produces
366 one of the largest lateral gradients in productivity (and in turn particle flux) in the world
367 (Behrenfeld and Falkowski, 1997). Thus our finding supports the use of ^{230}Th -normalization to
368 reconstruct sediment fluxes within cited uncertainties (François et al., 2004).

369 Although we cannot directly estimate the magnitude of boundary scavenging for ^{231}Pa
370 because the lateral water column ^{231}Pa gradients are not discernible, we can use the ^{230}Th results
371 in conjunction with the particulate $^{231}\text{Pa}/^{230}\text{Th}$ xs data (Fig. 4F) to estimate the redistribution of
372 ^{231}Pa . The near-bottom $^{231}\text{Pa}/^{230}\text{Th}$ xs ratio of particulate material, $(\text{Pa}/\text{Th})_{\text{bottom}}$, should represent
373 the ratio of sinking flux for the two elements. If both elements were being buried at their

374 production rate by U decay, we would expect this ratio to be 0.093 (activity units, see dotted line,
375 Fig. 4F). Therefore the ratio of sinking flux to overlying production for ^{231}Pa , $(F/P)_{\text{Pa}}$, is
376 proportional to that of ^{230}Th , weighted by the deviation of the near-bottom particulate material
377 from the production ratio:

$$378 \quad (F/P)_{\text{Pa}} = (F/P)_{\text{Th}} * (\text{Pa/Th})_{\text{bottom}} / 0.093 \quad (\text{Eq. 2})$$

379 The average particulate $^{231}\text{Pa}/^{230}\text{Th}$ ratio of the two near bottom samples at GT10-09,
380 within about 100 m of the seafloor, is 0.18 (Fig. 4F). Using $(F/P)_{\text{Th}} = 1.4$ as calculated above, we
381 estimate that ^{231}Pa is being buried at 2.7 times its production in the overlying water column at
382 this site. While clearly a region of enhanced ^{231}Pa removal, this region will likely not account for
383 observed depletion of ^{231}Pa in deep North Atlantic sediment. High productivity areas such as
384 GT10-09, where boundary scavenging of ^{231}Pa is occurring, are likely only a small volumetric
385 percentage of the basin (Lippold et al., 2012b). This is indicated by the sharp decrease in
386 particulate $^{231}\text{Pa}/^{230}\text{Th}$ xs ratio between stations GT10-09 and GT10-10 (Fig. 4F). Nonetheless,
387 more detailed mapping of the extent of this type of enhanced ^{231}Pa burial on the North African
388 margin is required before its impact on the basin-wide Pa budget can be quantified (Burke et al.,
389 2011; Marchal et al., 2000).

390 *3.3 Bottom scavenging and ventilation: convoluted influences across the North Atlantic*

391 Both ^{231}Pa xs and ^{230}Th xs (Fig. 3) have negative concentration anomalies associated with
392 the high salinity waters of the Mediterranean Outflow Water (MOW, ~1 km depth at station
393 GT10-01, Fig. 1). This is expected due to the high particle load of MOW, a result of the
394 interaction of the flow of Mediterranean Water over the Gibraltar Strait and the Iberian margin
395 (McCave and Hall, 2002; Thorpe, 1972), which is known to enhance scavenging of ^{234}Th and
396 ^{228}Th (half-life 1.8 yrs, parent ^{228}Ra) (Schmidt, 2006). Unexpectedly, the low radionuclide

397 concentrations (causing negative deviations to a linear profile) appear to be advected along with
398 the flow of MOW to station GT10-03 and even to GT10-05 for ^{231}Pa xs, while the high particle
399 concentrations (on the basis of C_p , Fig. 3A) are not, i.e. the downstream effects are not
400 necessarily due to in-situ scavenging. There is a strong boundary in ^{231}Pa xs concentrations and
401 water mass age between GT10-05 and GT10-07 at 2 km depth (Fig. 3), indicating more recently
402 ventilated water to the north, making it difficult to separate the downstream effects of
403 specifically MOW from a large-scale influence of other NADW components. This is the first of
404 several examples of how ventilation and bottom scavenging combine to produce low
405 concentration anomalies in the water column radionuclide distributions.

406 Second, we look in more detail (Fig. 6) at the impact of the enhanced scavenging
407 observed at station GT11-16, also known as the TAG hydrothermal site (Rona, 1980; Rona et al.,
408 1984). Clearly, dissolved ^{230}Th xs and ^{231}Pa xs are removed from solution in the observed
409 hydrothermal plume around 3.3 km depth (Figs. 3B, 3D, 6). But it also appears that the low
410 concentration anomaly in the plume is dispersed by circulation to shallower depths in the water
411 column. The TAG concentration profile departs negatively for dissolved ^{230}Th xs at 2.1 km, and
412 for dissolved ^{231}Pa xs at 1.5 km. Furthermore, the low radionuclide concentrations appear to be
413 advected to sites west of the ridge. For both radionuclides at 2.5 km depth, concentrations at
414 GT11-14 are lower than they are to the west at GT11-12, opposite to the expected trend due to
415 water mass ageing.

416 Westward and shoaling propagation of the hydrothermal scavenging anomaly is
417 consistent with theory, i.e. buoyant plume water rising and heading west due to geostrophic
418 considerations (Speer, 1989). We note that this type of hydrothermal circulation will not be
419 accounted for in the mean age estimates. This type of “downstream” hydrothermal effects (both

420 vertical and lateral, Fig. 6) are not caused only by the observed venting at the TAG site but are
421 more likely the integrated result of vent sites all along the ridge (German et al., 2010). This result
422 is support for the hypothesis that hydrothermal vents are a basin-scale sink of Pa in the deep
423 ocean (Hayes et al., 2013). However, because the observed hydrothermal anomaly and its far-
424 field effect occur in a region with strong zonal and meridional gradients in water mass age, it is
425 difficult to remove the influence of ventilation and isolate the hydrothermal scavenging
426 magnitude. For instance, one could estimate the removal flux of ^{231}Pa (or ^{230}Th) by using the
427 deficit of the observed concentration profile compared to a linear profile (expected due to
428 reversible scavenging) (Deng et al., 2014). The expected profile however cannot be chosen *a*
429 *priori*, because in a region of recent deep water ventilation one does not expect a linear profile.

430 Similarly, along Line W (GT11-01 thru GT11-10), dissolved ^{230}Th xs and ^{231}Pa xs
431 concentrations are clearly depleted near the bottom (Fig. 3B, D) due to increased particle
432 concentrations in nepheloid layers (Fig. 3A). Depletion of ^{230}Th and ^{231}Pa below 3.5 km depth
433 cannot be attributed to ventilation, the conventional explanation (e.g., Luo et al., 2010), because
434 ventilation time scales increase with depth below 3.5 km (Fig. 3E). Nonetheless, the fact that
435 ^{230}Th and ^{231}Pa concentrations at mid-depth (1-3km) along Line W, the depth range of maximum
436 southward NADW transport (Cunningham et al., 2007; Kanzow et al., 2010; Talley et al., 2003),
437 are much lower than at the corresponding depths in the eastern basin at GT11-20 and GT11-22
438 (Fig. 3B, D), where particle concentrations (C_p values) are similar to those along Line W (Fig.
439 3A), seems clearly related to the east-west gradient in mean age. Radionuclide depletions due to
440 bottom scavenging and recent ventilation again here seem convolved in a way that is difficult to
441 untangle with static tracer observations.

442 In yet another combination of influences, dissolved ^{230}Th xs and ^{231}Pa xs concentrations
443 both decrease toward the bottom at GT11-20 and GT11-22 at ~4 km and 2.5 km depth,
444 respectively, where there is no evidence for increased particle concentrations or recent
445 ventilation. While the deep water in the Northeast Atlantic has been long isolated from the
446 atmosphere (>500 yrs), it may not have been this long since a significant scavenging event
447 occurred. The inflow of NEADW from the Vema and Romanche Fracture Zones occurs on a
448 timescale of 30 years based on radiocarbon distributions (Schlitzer et al., 1985). The mid-
449 Atlantic ridge is associated with enhanced turbulent mixing because of its complex topography
450 (Polzin et al., 1996) and with metalliferous sediments from hydrothermal activity. Both of these
451 factors could cause bottom scavenging of ^{230}Th and ^{231}Pa from water flowing through the gaps in
452 the ridge, the former via resuspension of sediments and the latter by the increased scavenging
453 efficiency of Fe-Mn oxides. A radionuclide depleted signal could then be advected northward,
454 carrying with it its scavenging history. While this scenario is highly speculative, such are the
455 possible interactions between deep water flow and bottom scavenging that need to be accounted
456 for in a fuller understanding of the marine cycling of ^{230}Th and ^{231}Pa .

457 *3.4 Apparent controls on seawater and sedimentary $^{231}\text{Pa}/^{230}\text{Th}$ ratios*

458 Sensitivity tests in a scavenging-circulation ocean model, which can vary bottom
459 scavenging intensity and ventilation timescales independently, may be able to resolve the
460 significance of each process in determining radionuclide distributions in the North Atlantic. This
461 uncertainty notwithstanding, it is informative to inspect the section of the dissolved $^{231}\text{Pa}/^{230}\text{Th}$
462 xs ratio (Fig. 3C) with a motivation to examine its proxy applications. High ratios along the
463 Cape Verde transect are consistent with boundary scavenging as discussed in section 3.2. In the
464 areas of clear bottom scavenging along Line W and at the TAG hydrothermal site, the ratio is

465 also elevated above the corresponding mid-depth values. This is because the ^{230}Th is scavenged
466 more intensely (larger depletion from the dissolved phase) relative to ^{231}Pa at these locations. In
467 analogy to the boundary scavenging due to lateral gradients in scavenging intensity, the bottom
468 scavenging sites may also act as preferential sinks for Pa. Because of its longer residence time,
469 dispersive fluxes of Pa into the bottom scavenging sites likely result in a greater Pa burial rate
470 than would occur in the absence of bottom scavenging (Deng et al., 2014).

471 The impact of ventilation on the dissolved $^{231}\text{Pa}/^{230}\text{Th}$ xs distribution (Fig. 3C), however,
472 is not obvious. For instance, between 2-3 km depth (excluding GT11-16) the $^{231}\text{Pa}/^{230}\text{Th}$ ratio
473 changes very little between 500 and 4200 km section distance (Fig. 3C), along which the mean
474 age has a strong lateral gradient between roughly 80 yrs in the west and 400 yrs in the east. This
475 range in age is the exact time period in which one expects the strongest return to a steady-state of
476 ^{231}Pa concentrations after ventilation (Gherardi et al., 2010), according to a 1-dimensional
477 mixing-scavenging model (Moran et al., 2001; Rutgers v. d. Loeff and Berger, 1993). The
478 dissolved $^{231}\text{Pa}/^{230}\text{Th}$ xs ratio of course increases further toward the African margin as ventilation
479 age also increases, but this is primarily due to the stronger removal of dissolved ^{230}Th xs
480 (boundary scavenging, sec. 3.2) at the eastern margin.

481 The observed zonal gradient in dissolved $^{231}\text{Pa}/^{230}\text{Th}$ xs (Fig. 3C) is not consistent with
482 removal of ^{231}Pa by southward flow between 2-3 km depth, which one expects to be strongest in
483 the west (Wunsch and Heimbach, 2006, 2013). That said, we cannot refute that the large-scale
484 deficit of ^{231}Pa in North Atlantic sediments (Lippold et al., 2012a; Yu et al., 1996) is consistent
485 with some amount of zonally-integrated southward ^{231}Pa transport from the North Atlantic to the
486 South Atlantic. This interpretation is supported by our particulate $^{231}\text{Pa}/^{230}\text{Th}$ xs data being
487 mostly below the production ratio (Fig. 4F) and by transport analysis of recent water column data

488 from the South Atlantic (Deng et al., 2014). Whether the $^{231}\text{Pa}/^{230}\text{Th}$ distribution (as opposed to
489 ^{231}Pa itself) is also responding to a zonally integrated southward flow of NADW remains to be
490 demonstrated in a 3-D dimensional circulation-scavenging model.

491 For instance, in the deep basins (4-6 km depth), likely not influenced by the African
492 margin processes, the dissolved $^{231}\text{Pa}/^{230}\text{Th}$ xs ratio is higher on the eastern side of the mid-
493 Atlantic ridge, as expected from the trend in mean age (Fig. 3D), perhaps reflecting the
494 integrated removal of ^{231}Pa (relative to ^{230}Th) by southward flow throughout the water column.
495 Additionally, the ratio decreases with depth (below 1 km and away from bottom scavenging
496 sites), most significantly at the deep central basin stations GT11-12 and GT11-20. The decrease
497 with depth of the $^{231}\text{Pa}/^{230}\text{Th}$ ratio in the Atlantic has been suggested to reflect the southward
498 export of ^{231}Pa by deep water circulation (Lippold et al., 2011; Luo et al., 2010) based on 2-
499 dimensional ocean models which average out the east-west gradient in ventilation observed in
500 our transect (Fig. 3E), also suggesting a zonally-integrated effect of ventilation.

501 The influence of circulation may interestingly be more significant in the upper 1-1.2 km.
502 High $^{231}\text{Pa}/^{230}\text{Th}$ xs ratios near the surface are consistent with ^{230}Th being more intensely
503 scavenged out of the mixed layer, but a secondary subsurface maximum in dissolved $^{231}\text{Pa}/^{230}\text{Th}$
504 xs ratio around 1 km depth is observed at nearly every station. In the section between the mid-
505 ocean ridge and Mauritania, the secondary dissolved $^{231}\text{Pa}/^{230}\text{Th}$ xs maximum overlaps with
506 AAIW (cf. Fig. 1). The persistence of the $^{231}\text{Pa}/^{230}\text{Th}$ maximum in the more northern parts of the
507 transect, however, does not support an association with AAIW. An alternative scenario is that a
508 high $^{231}\text{Pa}/^{230}\text{Th}$ ratios throughout shallow water (0-1200 m), related to more intense scavenging
509 of ^{230}Th , is overprinted with the strong minimum around 500 m depth which could be related to
510 the low ^{231}Pa content and rapid ventilation of EDW. Yet another possible scenario is that the

511 subsurface dissolved $^{231}\text{Pa}/^{230}\text{Th}$ xs maximum is related to the preferential regeneration of
512 dissolved ^{231}Pa released during diatom dissolution (since biogenic opal is a strong scavenger of
513 ^{231}Pa (Chase et al., 2002)). This is not supported, however, by either the silicic acid distribution
514 (except within AAIW, Fig. 7B) or the particulate opal distribution (Lam et al., submitted). In any
515 case, the possibility of ^{231}Pa (and perhaps $^{231}\text{Pa}/^{230}\text{Th}$) tracing shallow or intermediate water
516 circulation is worth further attention since its longer-lived removal timescale and uniform
517 production offers a complement to the traditional transient tracers of shallow circulation (^3H - ^3He ,
518 CFC's).

519 As a way of summarizing these observations we cross-plot the dissolved $^{231}\text{Pa}/^{230}\text{Th}$ xs
520 data with another potential circulation tracer measured on the same water samples, silicic acid.
521 The silicic acid distribution along our transect (Fig. 7B) has a resemblance to the inverse
522 estimates of mean age (Fig. 3E). Silicic acid is added to deep water through the dissolution of
523 diatom opal exported from surface water and accumulates with deep water age (Broecker and
524 Peng, 1982). Furthermore, its distribution is sensitive to the overturning circulation since NADW
525 has very low (preformed) silicic acid and southern-sourced waters (AABW and AAIW) have
526 much higher end-member concentrations (Sarmiento et al., 2007). There is a wide scatter in the
527 relationship between dissolved $^{231}\text{Pa}/^{230}\text{Th}$ xs and silicic acid (Fig. 7A) and the overall negative
528 trend reflects that fact the $^{231}\text{Pa}/^{230}\text{Th}$ ratio generally decreases with depth while silicic acid (and
529 mean age) increase with depth. At some given depths (color scheme of points in Fig. 7A),
530 however, $^{231}\text{Pa}/^{230}\text{Th}$ may be positively related with silicic acid. For instance, around 1 km depth
531 (dark blue points in Fig. 7A) a positive trend possibly related to the influence of AAIW can be
532 seen. Some of the high $^{231}\text{Pa}/^{230}\text{Th}$ values at 3-4 km depth, however, are related to locations of
533 bottom scavenging (marked in Fig. 7A) and therefore cannot be ascribed to water mass ageing.

534 While a basin-scale, integrated influence of the southward export of NADW cannot be
535 ruled out, the distribution of dissolved $^{231}\text{Pa}/^{230}\text{Th}$ appears to be insensitive to water mass age
536 across the North Atlantic. In order to validate the use of the $^{231}\text{Pa}/^{230}\text{Th}$ ratio as a quantitative
537 paleo-indicator of the AMOC, a more complex conceptual model needs to be developed,
538 including the influences of boundary scavenging and bottom scavenging demonstrated here.

539 **4. Summary**

540 The cycling of ^{230}Th and ^{231}Pa in the ocean is complex. Deviations from the behavior
541 expected from a simple model of reversible scavenging are apparent across the North Atlantic
542 and improved spatial resolution allows us to study them in greater detail than has been done
543 before. Boundary scavenging of ^{230}Th in an exceptionally productive region off Northwest
544 Africa can be constrained to $40 \pm 10\%$ of its water column production, helping to quantify the
545 uncertainties associated with ^{230}Th -normalized sediment fluxes. Enhanced removal of ^{231}Pa
546 occurs on the Africa margin as well but quantitative conclusions about the significance of this
547 sink in the basin-scale Pa budget cannot be made without more detailed mapping of the region.
548 Both recent ventilation and bottom scavenging cause deep-water depletions of ^{230}Th and ^{231}Pa .
549 The dissolved $^{231}\text{Pa}/^{230}\text{Th}$ ratio traces locations of intense scavenging intensity while its
550 distribution in the transect is not consistent with a simple relationship to water-mass age. We
551 observe several examples where the effects of scavenging and ventilation are convolved which
552 provide excellent test cases for sensitivity studies of removal mechanisms in future ocean
553 modeling of these isotopes. Circulation and scavenging affect many trace metals of
554 biogeochemical and paleoceanographic interest (e.g. Fe, Co, Al), and thus further constraining
555 the cycling of ^{230}Th and ^{231}Pa will be of broad appeal in the oceanographic community.

556

557 **Acknowledgements**

558 Funding for ship time, sampling operations, and hydrographic data was provided by the U. S.
559 National Science Foundation to the US GEOTRACES North Atlantic Transect Management
560 team of W. Jenkins (OCE-0926423), E. Boyle (OCE-0926204), and G. Cutter (OCE-0926092).
561 Radionuclide studies were supported by NSF (OCE-0927064 to L-DEO, OCE-0926860 to
562 WHOI, OCE-0927757 to URI, and OCE-0927754 to UMN). LFR was also supported by Marie
563 Curie Reintegration Grant and the European Research Council. The crew of the R/V *Knorr*, the
564 Ocean Data Facility team (Mary Johnson, Rob Palomares, Susan Becker, Melissa Miller and
565 Courtney Schatzman), and the science team samplers for Niskin bottles and in situ pumps
566 (Katharina Pahnke, Brett Longworth, Paul Morris, Daniel Ohnemus, Kuanbo Zhou, Sylvain
567 Rigaud and Stephanie Owens) are all acknowledged for their critical roles in the success of these
568 cruises. On-shore analysis efforts of Maureen Auro, Joanne Boudreau, and the WHOI Plasma
569 Facility are greatly appreciated. Figures 1, 3 and 7 were created using Ocean Data View
570 (Schlitzer, 2011). We thank Alex Thomas and an anonymous reviewer for improving the quality
571 of the manuscript.

572

573

574

References

575

576 Andersen, M.B., Stirling, C.H., Zimmermann, B., Halliday, A.N., 2010. Precise determination of the open
577 ocean $^{234}\text{U}/^{238}\text{U}$ composition. *Geochem. Geophys. Geosyst.* 11, Q12003.

578 Anderson, R.F., 1982. Concentration, vertical flux, and remineralization of particulate uranium in
579 seawater. *Geochim. Cosmochim. Acta* 46, 1293-1299.

580 Anderson, R.F., Bacon, M.P., Brewer, P.G., 1983. Removal of ^{230}Th and ^{231}Pa at ocean margins. *Earth*
581 *Planet. Sci. Lett.* 66, 73-90.

582 Anderson, R.F., Fleisher, M.Q., Biscaye, P.E., Kumar, N., Dittrich, B., Kubik, P., Suter, M., 1994.
583 Anomalous boundary scavenging in the Middle Atlantic Bight: evidence from ^{230}Th , ^{231}Pa , ^{10}Be and ^{210}Pb .
584 *Deep Sea Res. Pt. II* 41, 537-561.

585 Anderson, R.F., Fleisher, M.Q., Robinson, L.F., Edwards, R.L., Hoff, J., Moran, S.B., Rutgers van der
586 Loeff, M.M., Thomas, A.L., Roy-Barman, M., François, R., 2012. GEOTRACES intercalibration of
587 ^{230}Th , ^{232}Th , ^{231}Pa , and prospects for ^{10}Be . *Limnol. Oceanogr. Methods* 10, 179-213.

588 Anderson, R.F., Lao, Y., Broecker, W.S., Trumbore, S.E., Hofmann, H.J., Wolfli, W., 1990. Boundary
589 scavenging in the Pacific Ocean: a comparison of ^{10}Be and ^{231}Pa . *Earth Planet. Sci. Lett.* 96, 287-304.

590 Auro, M.E., Robinson, L.F., Burke, A., Bradtmiller, L.I., Fleisher, M.Q., Anderson, R.F., 2012.
591 Improvements to ^{232}Th -thorium, ^{230}Th -thorium, and ^{231}Pa -protactinium analysis in seawater arising from
592 GEOTRACES intercalibration. *Limnol. Oceanogr.: Methods* 10, 464-474.

- 593 Bacon, M.P., 1984. Glacial to interglacial changes in carbonate and clay sedimentation in the Atlantic
594 Ocean estimated from ^{230}Th measurements. *Chem. Geol.* 46, 97-111.
- 595 Bacon, M.P., 1988. Tracers of chemical scavenging in the ocean: boundary effects and large-scale
596 chemical fractionation. *Philos. Trans. R. Soc. London, Ser. A* 325, 147-160.
- 597 Bacon, M.P., Anderson, R.F., 1982. Distribution of thorium isotopes between dissolved and particulate
598 forms in the deep sea. *J. Geophys. Res.* 87, 2045-2056.
- 599 Bacon, M.P., Rutgers v. d. Loeff, M.M., 1989. Removal of thorium-234 by scavenging in the bottom
600 nepheloid layer of the ocean. *Earth Planet. Sci. Lett.* 92, 157-164.
- 601 Bacon, M.P., Spencer, D.W., Brewer, P.G., 1976. $^{210}\text{Pb}/^{226}\text{Ra}$ and $^{210}\text{Po}/^{210}\text{Pb}$ disequilibria in seawater and
602 suspended particulate matter. *Earth Planet. Sci. Lett.* 32, 277-296.
- 603 Baker, E.T., Lavelle, J.W., 1984. The effect of particle size on the light attenuation coefficient of natural
604 suspensions. *J. Geophys. Res.: Oceans* 89, 8197-8203.
- 605 Behrenfeld, M.J., Falkowski, P.G., 1997. Photosynthetic rates derived from satellite-based chlorophyll
606 concentration. *Limnol. Oceanogr.* 42, 1-20.
- 607 Biscaye, P.E., Eittrheim, S.L., 1977. Suspended particulate loads and transports in the nepheloid layer of
608 the abyssal Atlantic Ocean. *Mar. Geol.* 23, 155-172.
- 609 Bishop, J.K., Lam, P.J., Wood, T.J., 2012. Getting good particles: Accurate sampling of particles by large
610 volume in-situ filtration. *Limnol. Oceanogr.: Methods* 10, 681-710.
- 611 Bishop, J.K.B., 1986. The correction and suspended particulate matter calibration of Sea Tech
612 transmissometer data. *Deep Sea Res. Pt. A* 33, 121-134.
- 613 Brewer, P.G., Spencer, D.W., Biscaye, P.E., Hanley, A., Sachs, P.L., Smith, C.L., Kadar, S., Fredericks,
614 J., 1976. The distribution of particulate matter in the Atlantic Ocean. *Earth Planet. Sci. Lett.* 32, 393-402.
- 615 Broecker, W., 2008. Excess sediment ^{230}Th : Transport along the sea floor or enhanced water column
616 scavenging? *Global Biogeochem. Cycles* 22, GB1006.
- 617 Broecker, W.S., Blanton, S., Smethie, W.M., Ostlund, G., 1991. Radiocarbon decay and oxygen
618 utilization in the Deep Atlantic Ocean. *Global Biogeochem. Cycles* 5, 87-117.
- 619 Broecker, W.S., Peng, T.-H., 1982. *Tracers in the Sea*. Lamont-Doherty Geol. Obs., Palisades, NY.
- 620 Broecker, W.S., Takahashi, T., Stuiver, M., 1980. Hydrography of the central Atlantic—II waters beneath
621 the Two-Degree Discontinuity. *Deep Sea Res. Pt. A* 27, 397-419.

- 622 Bruland, K., Lohan, M., 2003. Controls of Trace Metals in Seawater. *Treatise on Geochemistry* 6, 23-47.
- 623 Burke, A., Marchal, O., Bradtmiller, L.I., McManus, J.F., François, R., 2011. Application of an inverse
624 method to interpret $^{231}\text{Pa}/^{230}\text{Th}$ observations from marine sediments. *Paleoceanography* 26, PA1212.
- 625 Chase, Z., Anderson, R.F., Fleisher, M.Q., Kubik, P.W., 2002. The influence of particle composition and
626 particle flux on scavenging of Th, Pa and Be in the ocean. *Earth Planet. Sci. Lett.* 204, 215-229.
- 627 Cheng, H., Edwards, R.L., Hoff, J., Gallup, C.D., Richards, D.A., Asmerom, Y., 2000. The half-lives of
628 uranium-234 and thorium-230. *Chem. Geol.* 169, 17-33.
- 629 Cunningham, S.A., Kanzow, T., Rayner, D., Baringer, M.O., Johns, W.E., Marotzke, J., Longworth, H.R.,
630 Grant, E.M., Hirschi, J.J.-M., Beal, L.M., Meinen, C.S., Bryden, H.L., 2007. Temporal Variability of the
631 Atlantic Meridional Overturning Circulation at 26.5°N. *Science* 317, 935-938.
- 632 Delanghe, D., Bard, E., Hamelin, B., 2002. New TIMS constraints on the uranium-238 and uranium-234
633 in seawaters from the main ocean basins and the Mediterranean Sea. *Mar. Chem.* 80, 79-93.
- 634 DeMaster, D.J., Brewster, D.C., McKee, B.A., Nittrouer, C.A., 1991. Rates of particle scavenging,
635 sediment reworking, and longitudinal ripple formation at the HEBBLE site based on measurements of
636 ^{234}Th and ^{210}Pb . *Mar. Geol.* 99, 423-444.
- 637 Deng, F., Thomas, A.L., Rijkenberg, M.J.A., Henderson, G.M., 2014. Controls on seawater ^{231}Pa , ^{230}Th
638 and ^{232}Th concentrations along the flow paths of deep waters in the Southwest Atlantic. *Earth Planet. Sci.*
639 *Lett.* 390, 93-102.
- 640 François, R., Bacon, M.P., Suman, D.O., 1990. Thorium-230 profiling in deep-sea sediments: High-
641 resolution records of flux and dissolution of carbonate in the equatorial Atlantic during the last 24,000
642 years. *Paleoceanography* 5, 761-787.
- 643 François, R., Frank, M., Rutgers van der Loeff, M., Bacon, M.P., Geibert, W., Kienast, S., Anderson,
644 R.F., Bradtmiller, L., Chase, Z., Henderson, G., 2007. Comment on "Do geochemical estimates of
645 sediment focusing pass the sediment test in the equatorial Pacific?" by M. Lyle et al. *Paleoceanography*
646 22.
- 647 François, R., Frank, M., Rutgers van der Loeff, M.M., Bacon, M.P., 2004. ^{230}Th normalization: An
648 essential tool for interpreting sedimentary fluxes during the late Quaternary. *Paleoceanography* 19,
649 PA1018.
- 650 Gardner, W.D., Biscaye, P.E., Zaneveld, J.R.V., Richardson, M.J., 1985. Calibration and comparison of
651 the LDGO nephelometer and the OSU transmissometer on the Nova Scotian rise. *Mar. Geol.* 66, 323-344.
- 652 German, C.R., Fleer, A.P., Bacon, M.P., Edmond, J.M., 1991. Hydrothermal scavenging at the Mid-
653 Atlantic Ridge: radionuclide distributions. *Earth Planet. Sci. Lett.* 105, 170-181.

- 654 German, C.R., Higgs, N.C., Thomson, J., Mills, R., Elderfield, H., Blusztajn, J., Flerer, A.P., Bacon, M.P.,
655 1993. A geochemical study of metalliferous sediment from the TAG Hydrothermal Mound, 26°08'N,
656 Mid-Atlantic Ridge. *J. Geophys. Res.: Solid Earth* 98, 9683-9692.
- 657 German, C.R., Thurnherr, A.M., Knoery, J., Charlou, J.L., Jean-Baptiste, P., Edmonds, H.N., 2010. Heat,
658 volume and chemical fluxes from submarine venting: A synthesis of results from the Rainbow
659 hydrothermal field, 36°N MAR. *Deep Sea Res. Pt. I* 57, 518-527.
- 660 Gherardi, J.M., Luo, Y., Francois, R., McManus, J.F., Allen, S.E., Labeyrie, L., 2010. Reply to comment
661 by S. Peacock on “Glacial-interglacial circulation changes inferred from ²³¹Pa/²³⁰Th sedimentary record in
662 the North Atlantic region”. *Paleoceanography* 25, PA2207.
- 663 Hayes, C.T., Anderson, R.F., Jaccard, S.L., François, R., Fleisher, M.Q., Soon, M., Gersonde, R., 2013. A
664 new perspective on boundary scavenging in the North Pacific Ocean. *Earth Planet. Sci. Lett.* 369-370, 86-
665 97.
- 666 Henderson, G.M., Anderson, R.F., 2003. The U-series Toolbox for Paleoceanography. *Rev. Mineral.*
667 *Geochem.* 52, 493-531.
- 668 Henderson, G.M., Heinze, C., Anderson, R.F., Winguth, A.M.E., 1999. Global distribution of the ²³⁰Th
669 flux to ocean sediments constrained by GCM modelling. *Deep Sea Res. Pt. I* 46, 1861-1893.
- 670 Jenkins, W.J., 1988. The Use of Anthropogenic Tritium and Helium-3 to Study Subtropical Gyre
671 Ventilation and Circulation. *Phil. Trans. R. Soc. London, Ser. A* 325, 43-61.
- 672 Kanzow, T., Cunningham, S.A., Johns, W.E., Hirschi, J.J.M., Marotzke, J., Baringer, M.O., Meinen, C.S.,
673 Chidichimo, M.P., Atkinson, C., Beal, L.M., Bryden, H.L., Collins, J., 2010. Seasonal Variability of the
674 Atlantic Meridional Overturning Circulation at 26.5°N. *J. Clim.* 23, 5678-5698.
- 675 Khatiwala, S., Primeau, F., Holzer, M., 2012. Ventilation of the deep ocean constrained with tracer
676 observations and implications for radiocarbon estimates of ideal mean age. *Earth Planet. Sci. Lett.* 325–
677 326, 116-125.
- 678 Krishnaswami, S., Lal, D., Somayajulu, B.L.K., Weiss, R.F., Craig, H., 1976. Large-volume in-situ
679 filtration of deep Pacific waters: Mineralogical and radioisotope studies. *Earth Planet. Sci. Lett.* 32, 420-
680 429.
- 681 Lam, P.J., Morris, P.J., 2013. In situ marine sample collection system and methods, US Non Provisional
682 Patent Application No. 13/864,655. Patent Pending, submitted April 17, 2013.
- 683 Lam, P.J., Ohnemus, D.C., Auro, M.E., submitted. Size fractionated major particle composition and mass
684 from the US GEOTRACES North Atlantic Zonal Transect. *Deep Sea Res, Pt. II.*
- 685 Lao, Y., Anderson, R.F., Broecker, W.S., 1992. Boundary scavenging and deep-sea sediment dating:
686 constraints from excess ²³⁰Th and ²³¹Pa. *Paleoceanography* 7, 783-798.

- 687 LeBel, D.A., Smethie Jr, W.M., Rhein, M., Kieke, D., Fine, R.A., Bullister, J.L., Min, D.-H., Roether, W.,
688 Weiss, R.F., Andri , C., Smythe-Wright, D., Peter Jones, E., 2008. The formation rate of North Atlantic
689 Deep Water and Eighteen Degree Water calculated from CFC-11 inventories observed during WOCE.
690 Deep Sea Res. Pt. I 55, 891-910.
- 691 Ledwell, J.R., Watson, A.J., Law, C.S., 1998. Mixing of a tracer in the pycnocline. J. Geophys. Res.:
692 Oceans 103, 21499-21529.
- 693 Legeleux, F., Reyss, J.-L., Floris, S., 1995. Entrainement des metaux vers les sediments sur les marges
694 continentales de l'Atlantic Est. C. R. Acad. Sci. Paris 320 (serie IIA), 1195-1202.
- 695 Lippold, J., Gherardi, J.-M., Luo, Y., 2011. Testing the $^{231}\text{Pa}/^{230}\text{Th}$ paleocirculation proxy: A data versus
696 2D model comparison. Geophys. Res. Lett. 38, L20603.
- 697 Lippold, J., Luo, Y., Francois, R., Allen, S.E., Gherardi, J., Pichat, S., Hickey, B., Schulz, H., 2012a.
698 Strength and geometry of the glacial Atlantic Meridional Overturning Circulation. Nature Geosci. 5, 813-
699 816.
- 700 Lippold, J., Mulitza, S., Mollenhauer, G., Weyer, S., Heslop, D., Christl, M., 2012b. Boundary
701 scavenging at the East Atlantic margin does not negate use of $^{231}\text{Pa}/^{230}\text{Th}$ to trace Atlantic overturning.
702 Earth Planet. Sci. Lett. 333–334, 317-331.
- 703 Luo, Y., Francois, R., Allen, S.E., 2010. Sediment $^{231}\text{Pa}/^{230}\text{Th}$ as a recorder of the rate of the Atlantic
704 meridional overturning circulation: insights from a 2-D model. Ocean Sciences 6, 381-400.
- 705 Lyle, M., Mitchell, N., Pisias, N., Mix, A., Martinez, J.I., Paytan, A., 2005. Do geochemical estimates of
706 sediment focusing pass the sediment test in the equatorial Pacific? Paleoceanography 20, PA1005.
- 707 Lyle, M., Pisias, N., Paytan, A., Martinez, J.I., Mix, A., 2007. Reply to comment by R. Francois et al. on
708 “Do geochemical estimates of sediment focusing pass the sediment test in the equatorial Pacific?”:
709 Further explorations of ^{230}Th normalization. Paleoceanography 22, PA1217.
- 710 Mangini, A., Diester-Haas, L., 1983. Excess Th-230 in sediments off NW Africa traces upwelling in the
711 past, in: Thiede, J., Suess, E. (Eds.), Coastal upwelling: Its Sediment Record (Part A). Plenum Press, New
712 York, pp. 455-470.
- 713 Marchal, O., Francois, R., Stocker, T.F., Joos, F., 2000. Ocean thermohaline circulation and sedimentary
714 $^{231}\text{Pa}/^{230}\text{Th}$ ratio. Paleoceanography 15, 625-641.
- 715 McCartney, M.S., Bennett, S.L., Woodgate-Jones, M.E., 1991. Eastward Flow through the Mid-Atlantic
716 Ridge at 11°N and Its Influence on the Abyss of the Eastern Basin. J. Phys. Oceanogr. 21, 1089-1121.
- 717 McCave, I.N., 1986. Local and global aspects of the bottom nepheloid layers in the world ocean. Neth. J.
718 Sea Res. 20, 167-181.

- 719 McCave, I.N., Hall, I.R., 2002. Turbidity of waters over the Northwest Iberian continental margin. *Prog. Oceanogr.* 52, 299-313.
720
- 721 McManus, J.F., Francois, R., Gherardi, J.M., Keigwin, L.D., Brown-Leger, S., 2004. Collapse and rapid
722 resumption of Atlantic meridional circulation linked to deglacial climate changes. *Nature* 428, 834-837.
- 723 Moran, S.B., Charette, M.A., Hoff, J.A., Edwards, R.L., Landing, W.M., 1997. Distribution of ^{230}Th in
724 the Labrador Sea and its relation to ventilation. *Earth Planet. Sci. Lett.* 150, 151-160.
- 725 Moran, S.B., Hoff, J.A., Buesseler, K.O., Edwards, R.L., 1995. High precision ^{230}Th and ^{232}Th in the
726 Norwegian Sea and Denmark by thermal ionization mass spectrometry. *Geophys. Res. Lett.* 22, 2589-
727 2592.
- 728 Moran, S.B., Shen, C., C, Weinstein, S.E., Hettinger, L.H., Hoff, J.H., Edmonds, H.N., Edwards, R.L.,
729 2001. Constraints on deep water age and particle flux in the equatorial and South Atlantic Ocean based on
730 seawater ^{231}Pa and ^{230}Th data. *Geophys. Res. Lett.* 28, 3437-3440.
- 731 Moran, S.B., Shen, C.C., Edmonds, H.N., Weinstein, S.E., Smith, J.N., Edwards, R.L., 2002. Dissolved
732 and particulate ^{231}Pa and ^{230}Th in the Atlantic Ocean: constraints on intermediate/deep water age,
733 boundary scavenging, and $^{231}\text{Pa}/^{230}\text{Th}$ fractionation. *Earth Planet. Sci. Lett.* 203, 999-1014.
- 734 Nozaki, Y., Horibe, Y., Tsubota, H., 1981. The water column distributions of thorium isotopes in the
735 western North Pacific. *Earth Planet. Sci. Lett.* 54, 203-216.
- 736 Nozaki, Y., Nakanishi, T., 1985. ^{231}Pa and ^{230}Th profiles in the open ocean water column. *Deep-Sea Res.*
737 *Pt. A* 32, 1209-1220.
- 738 Okubo, A., Obata, H., Gamo, T., Yamada, M., 2012. ^{230}Th and ^{232}Th distributions in mid-latitudes of the
739 North Pacific Ocean: Effect of bottom scavenging. *Earth Planet. Sci. Lett.* 339–340, 139-150.
- 740 Polzin, K.L., Speer, K.G., Toole, J.M., Schmitt, R.W., 1996. Intense mixing of Antarctic Bottom Water in
741 the equatorial Atlantic Ocean. *Nature* 380, 54-57.
- 742 Richardson, M.J., 1987. Particle size, light scattering and composition of suspended particulate matter in
743 the North Atlantic. *Deep Sea Res. Pt. A* 34, 1301-1329.
- 744 Robert, J., Miranda, C.F., Muxart, R., 1969. Mesure de la periode du protactinium-231 par
745 microcalorimetrie. *Radiochim. Acta* 11, 104-108.
- 746 Robinson, L.F., Belshaw, N.S., Henderson, G.M., 2004. U and Th concentrations and isotope ratios in
747 modern carbonates and waters from the Bahamas. *Geochim. Cosmochim. Acta* 68, 1777-1789.
- 748 Rona, P.A., 1980. TAG Hydrothermal Field: Mid-Atlantic Ridge crest at latitude 26°N. *J. Geol. Soc.*
749 *London* 137, 385-402.

- 750 Rona, P.A., Thompson, G., Mottl, M.J., Karson, J.A., Jenkins, W.J., Graham, D., Mallette, M., Von
751 Damm, K., Edmond, J.M., 1984. Hydrothermal activity at the Trans-Atlantic Geotraverse Hydrothermal
752 Field, Mid-Atlantic Ridge crest at 26°N. *J.f Geophys. Res.: Solid Earth* 89, 11365-11377.
- 753 Roy-Barman, M., 2009. Modelling the effect of boundary scavenging on thorium and protactinium
754 profiles in the ocean. *Biogeosciences* 6, 3091-3197.
- 755 Rutgers v. d. Loeff, M., Berger, G.W., 1993. Scavenging of ²³⁰Th and ²³¹Pa near the Antarctic polar front
756 in the South Atlantic. *Deep Sea Res. Pt. I* 40, 339-357.
- 757 Sarmiento, J.L., Simeon, J., Gnanadesikan, A., Gruber, N., Key, R.M., Schlitzer, R., 2007. Deep ocean
758 biogeochemistry of silicic acid and nitrate. *Global Biogeochem. Cycles* 21, GB1S90.
- 759 Schlitzer, R., 1987. Renewal rates of East Atlantic deep water estimated by inversion of ¹⁴C data. *J.*
760 *Geophys. Res.: Oceans* 92, 2953-2969.
- 761 Schlitzer, R., 2011. <http://odv.awi.de>.
- 762 Schlitzer, R., Roether, W., Weidmann, U., Kalt, P., Loosli, H.H., 1985. A meridional ¹⁴C and ³⁹Ar section
763 in northeast Atlantic deep water. *J. Geophys. Res.: Oceans* 90, 6945-6952.
- 764 Schmidt, S., 2006. Impact of the Mediterranean Outflow Water on particle dynamics in intermediate
765 waters of the Northeast Atlantic, as revealed by ²³⁴Th and ²²⁸Th. *Mar. Chem.* 100, 289-298.
- 766 Scholten, J.C., Fietzke, J., Mangini, A., Garbe-Schönberg, C.D., Eisenhauer, A., Schneider, R., Stoffers,
767 P., 2008. Advection and scavenging: Effects on ²³⁰Th and ²³¹Pa distribution off Southwest Africa. *Earth*
768 *Planet. Sci. Lett.* 271, 159-169.
- 769 Scholten, J.C., Fietzke, J., Vogler, S., Rutgers van der Loeff, M.M., Mangini, A., Koeve, W., Waniek, J.,
770 Stoffers, P., Antia, A., Kuss, J., 2001. Trapping efficiencies of sediment traps from the deep Eastern
771 North Atlantic: the ²³⁰Th calibration. *Deep Sea Res. Pt. II* 48, 2383-2408.
- 772 Shen, C.-C., Cheng, H., Edwards, R.L., Moran, S.B., Edmonds, H.N., Hoff, J.A., Thomas, R.B., 2003.
773 Measurement of Attogram Quantities of ²³¹Pa in Dissolved and Particulate Fractions of Seawater by
774 Isotope Dilution Thermal Ionization Mass Spectroscopy. *Anal. Chem.* 75, 1075-1079.
- 775 Shen, C.-C., Lawrence Edwards, R., Cheng, H., Dorale, J.A., Thomas, R.B., Bradley Moran, S.,
776 Weinstein, S.E., Edmonds, H.N., 2002. Uranium and thorium isotopic and concentration measurements
777 by magnetic sector inductively coupled plasma mass spectrometry. *Chem. Geol.* 185, 165-178.
- 778 Shen, C.-C., Wu, C.-C., Cheng, H., Lawrence Edwards, R., Hsieh, Y.-T., Gallet, S., Chang, C.-C., Li, T.-
779 Y., Lam, D.D., Kano, A., Hori, M., Spötl, C., 2012. High-precision and high-resolution carbonate ²³⁰Th
780 dating by MC-ICP-MS with SEM protocols. *Geochim. Cosmochim. Acta* 99, 71-86.

- 781 Shimmiel, G.B., Murray, J.W., Thomson, J., Bacon, M.P., Anderson, R.F., Price, N.B., 1986. The
782 distribution and behaviour of ^{230}Th and ^{231}Pa at an ocean margin, Baja California, Mexico. *Geochim.*
783 *Cosmochim. Acta* 50, 2499-2507.
- 784 Siddall, M., Anderson, R.F., Winckler, G., Henderson, G.M., Bradtmiller, L.I., McGee, D., Franzese, A.,
785 Stocker, T.F., Müller, S.A., 2008. Modeling the particle flux effect on distribution of ^{230}Th in the
786 equatorial Pacific. *Paleoceanography* 23, PA2208.
- 787 Singh, A.K., Marcantonio, F., Lyle, M., 2013. Water column ^{230}Th systematics in the eastern equatorial
788 Pacific Ocean and implications for sediment focusing. *Earth Planet. Sci. Lett.* 362, 294-304.
- 789 Speer, K.G., 1989. a forced baroclinic vortex around a hydrothermal plume. *Geophysical Research*
790 *Letters* 16, 461-464.
- 791 Spencer, D.W., Bacon, M.P., Brewer, P.G., 1981. Models of the distribution of ^{210}Pb in a section across
792 the North Equatorial Atlantic Ocean. *J. Mar. Res.* 39, 119-138.
- 793 Suman, D.O., Bacon, M.P., 1989. Variations in Holocene sedimentation in the North American Basin
794 determined from ^{230}Th measurements. *Deep Sea Res. Pt. A* 36, 869-878.
- 795 Talley, L.D., 1999. Some aspects of ocean heat transport by the shallow, intermediate and deep
796 overturning circulations, *Mechanisms of Global Climate Change at Millennial Time Scales*, *Geophys.*
797 *Monogr. Amer. Geophys. Union*, pp. 1-22.
- 798 Talley, L.D., Reid, J.L., Robbins, P.E., 2003. Data-Based Meridional Overturning Streamfunctions for the
799 Global Ocean. *J. Clim.* 16, 3213-3226.
- 800 Thorpe, S., 1972. A sediment cloud below the Mediterranean outflow. *Nature* 239, 326-327.
- 801 Toole, J.M., Curry, R.G., Joyce, T.M., McCartney, M., Peña-Molino, B., 2011. Transport of the North
802 Atlantic Deep Western Boundary Current about 39°N , 70°W : 2004–2008. *Deep Sea Res. Pt. II* 58, 1768-
803 1780.
- 804 Tsuchiya, M., 1989. Circulation of the Antarctic Intermediate Water in the North Atlantic Ocean. *J. Mar.*
805 *Res.* 47, 747-755.
- 806 Turnewitsch, R., Reyss, J.-L., Nycander, J., Waniek, J.J., Lampitt, R.S., 2008. Internal tides and sediment
807 dynamics in the deep sea—Evidence from radioactive $^{234}\text{Th}/^{238}\text{U}$ disequilibria. *Deep Sea Res. Pt. I* 55,
808 1727-1747.
- 809 Turnewitsch, R., Springer, B.M., 2001. Do bottom mixed layers influence ^{234}Th dynamics in the abyssal
810 near-bottom water column? *Deep Sea Res. Pt. I* 48, 1279-1307.
- 811 Venchiarutti, C., Jeandel, C., Roy-Barman, M., 2008. Particle dynamics study in the wake of Kerguelen
812 Island using thorium isotopes. *Deep Sea Res. Pt. I* 55, 1343-1363.

- 813 Vogler, S., Scholten, J., Rutgers van der Loeff, M., Mangini, A., 1998. ^{230}Th in the eastern North Atlantic:
814 the importance of water mass ventilation in the balance of ^{230}Th . *Earth Planet. Sci. Letters* 156, 61-74.
- 815 Walter, H.-J., Rutgers v. d. Loeff, M.M., Francois, R., 1999. Reliability of the $^{231}\text{Pa}/^{230}\text{Th}$ Activity Ratio
816 as a Tracer for Bioproductivity of the Ocean, in: Fischer, W., Wefer, G. (Eds.), *Use of Proxies in*
817 *Paleoceanography: Examples for the South Atlantic*. Springer-Verlag, Berlin, pp. 393-408.
- 818 Weyer, S., Anbar, A.D., Gerdes, A., Gordon, G.W., Algeo, T.J., Boyle, E.A., 2008. Natural fractionation
819 of $^{238}\text{U}/^{235}\text{U}$. *Geochim. Cosmochim. Acta* 72, 345-359.
- 820 Wunsch, C., Heimbach, P., 2006. Estimated Decadal Changes in the North Atlantic Meridional
821 Overturning Circulation and Heat Flux 1993–2004. *J. Phys. Oceanogr.* 36, 2012-2024.
- 822 Wunsch, C., Heimbach, P., 2013. Two Decades of the Atlantic Meridional Overturning Circulation:
823 Anatomy, Variations, Extremes, Prediction, and Overcoming Its Limitations. *J. Climate* 26, 7167-7186.
- 824 Yang, H.-S., Nozaki, Y., Sakai, H., Masuda, A., 1986. The distribution of ^{230}Th and ^{231}Pa in the deep-sea
825 surface sediments of the Pacific Ocean. *Geochim. Cosmochim. Acta* 50, 81-89.
- 826 Yu, E.-F., Francois, R., Bacon, M.P., 1996. Similar rates of modern and last-glacial ocean thermohaline
827 circulation inferred from radiochemical data. *Nature* 379, 689-694.
- 828 Yu, E.-F., Francois, R., Bacon, M.P., Fleer, A.P., 2001. Fluxes of ^{230}Th and ^{231}Pa to the deep sea:
829 implications for the interpretation of excess ^{230}Th and $^{231}\text{Pa}/^{230}\text{Th}$ profiles in sediments. *Earth Planet. Sci.*
830 *Lett.* 191, 219-230.
- 831 Zenk, W., Klein, B., Schroder, M., 1991. Cape Verde Frontal Zone. *Deep Sea Res. Pt. A* 38, Supplement
832 1, S505-S530.
833
834
835

836 **Figure Captions**

837 **Figure 1** Map of GEOTRACES section GA03, the U.S. GEOTRACES North Atlantic Transect
838 and section of salinity as measured in the Niskin bottle rosette casts. Neutral density overlays
839 define, in order of increasing density, the bottom of Eighteen Degree Water (EDW), Upper and
840 Classic Labrador Sea Water (ULSW/CLSW), Iceland-Scotland Overflow Water (ISOW),
841 Denmark-Strait Overflow Water (DSOW) and Antarctic Bottom Water (AABW), defined largely
842 for the western basin by Toole et al. (2010) and LeBel et al. (2008). The deep (>3 km) eastern
843 basin is filled with a more homogeneous water mass named Northeast Atlantic Deep Water
844 (NEADW) (Schlitzer et al., 1985). The southeastern section is influenced by Antarctic
845 Intermediate Water (AAIW) at about ~1 km depth and the northeastern margin is clearly
846 influenced by the high salinity Mediterranean Outflow Water (MOW). Presented in this paper is
847 dissolved radionuclide data for all stations listed here, and a sub-set of particulate radionuclide
848 data for stations marked with a black diamond.

849
850 **Figure 2.** Schematic representation of boundary scavenging. Along distance from an ocean
851 margin, particle flux (in arbitrary units, a.u.) increases nearly exponentially. The particulate and
852 dissolved $^{231}\text{Pa}/^{230}\text{Th}$ ratio are expected to increase with increasing particle flux, associated with
853 increasing scavenging intensity. Note that the particulate $^{231}\text{Pa}/^{230}\text{Th}$ ratios overlap the
854 production activity ratio (A.R., 0.093) produced from uranium decay, whereas the dissolved
855 ratios are roughly 10 times higher due to the preferential scavenging of ^{230}Th from seawater. The
856 longer residence time of ^{231}Pa , compared to that of ^{230}Th , allows a greater lateral flux of ^{231}Pa
857 down the concentration gradient toward the margin. This results in increased sinking vertical flux
858 of ^{231}Pa at the margin, at the expense of a lower vertical flux in the ocean interior. In contrast, the
859 sinking ^{230}Th flux is relatively uniform since its lateral movement is more limited. Therefore the
860 water column sustains greater lateral concentration gradients in ^{230}Th than in ^{231}Pa . The
861 numerical values used here are simply for illustration and do not represent actual observations.

862
863 **Figure 3** Property sections of the US GEOTRACES North Atlantic transect. (A) Particle beam
864 attenuation coefficient, C_p , determined by transmissometer. CTD casts are marked in black. (B)
865 Dissolved (<0.45 μm) ^{230}Th , (C) $^{231}\text{Pa}/^{230}\text{Th}$ activity ratio, and (D) ^{231}Pa . Black dots indicate
866 discrete measurements. (E) Mean age of seawater since being at the surface as estimated by
867 Khatiwala et al. (2012). Station locations for radionuclide data are as labeled in the map of
868 Figure 1. Panels A and E, in addition, have data from shallow “demi” stations occupied in
869 between full depth stations, as plotted in the inset map of panel E. See Fig. 1 for neutral density
870 surfaces not included here for clarity.

871
872 **Figure 4** Depth profiles of particulate (0.45-51 μm) (A, B) and total (C, D) ^{230}Th xs and ^{231}Pa xs
873 and the dissolved (<0.45 μm) (E) and particulate (F) $^{231}\text{Pa}/^{230}\text{Th}$ xs ratio from stations along a
874 zonal transect between Mauritania and west of Cape Verde. The dashed lines in (E) and (F)
875 represent the activity ratio of $^{231}\text{Pa}/^{230}\text{Th}$ produced by uranium decay (0.093). Legend relates
876 station names as located in Figure 1.

877
878 **Figure 5** (A) Depth profiles of total ^{230}Th interpolated onto a common set of isopycnal surfaces.
879 (B) Discretely calculated lateral concentration gradients in total ^{230}Th . Units are $\mu\text{Bq} \times 10^{-3}$ per
880 kilogram seawater per kilometer distance (C) Discretely calculated second lateral concentration

881 gradient in total ^{230}Th . Units are $\mu\text{Bq} \times 10^{-6}$ per kilogram seawater per square kilometer (D)
882 Schematic demonstrating the concept of calculating lateral gradients using the concentration
883 difference between depth profiles and the distance separating the profile locations along the Cape
884 Verde transect.

885
886 **Figure 6** Depth profiles of dissolved ^{230}Th and ^{231}Pa from the hydrothermal TAG site, GT11-16,
887 and the surrounding stations. As inferred from the section (Fig. 3), it is possible that the strong
888 removal of both isotopes at hydrothermal plumes along the Mid-Atlantic Ridge causes
889 downstream radionuclide depletion, with respect to the linear increase in concentration with
890 depth expected from reversible scavenging, at sites to the west of the ridge (GT11-14 and GT11-
891 12) but not significantly to the east (GT11-18).

892
893 **Figure 7** (A) Dissolved $^{231}\text{Pa}/^{230}\text{Th}$ xs ratios versus silicic acid measured in the same samples.
894 The arrow indicates a possible positive trend between $^{231}\text{Pa}/^{230}\text{Th}$ xs ratios and silicic acid carried
895 by Antarctic Intermediate Water (AAIW). The circled points represent locations of bottom
896 scavenging which causes elevated $^{231}\text{Pa}/^{230}\text{Th}$ xs ratios and are unrelated to the circulation
897 patterns traced by silicic acid. (B) Silicic acid distribution along the North Atlantic transect.

898

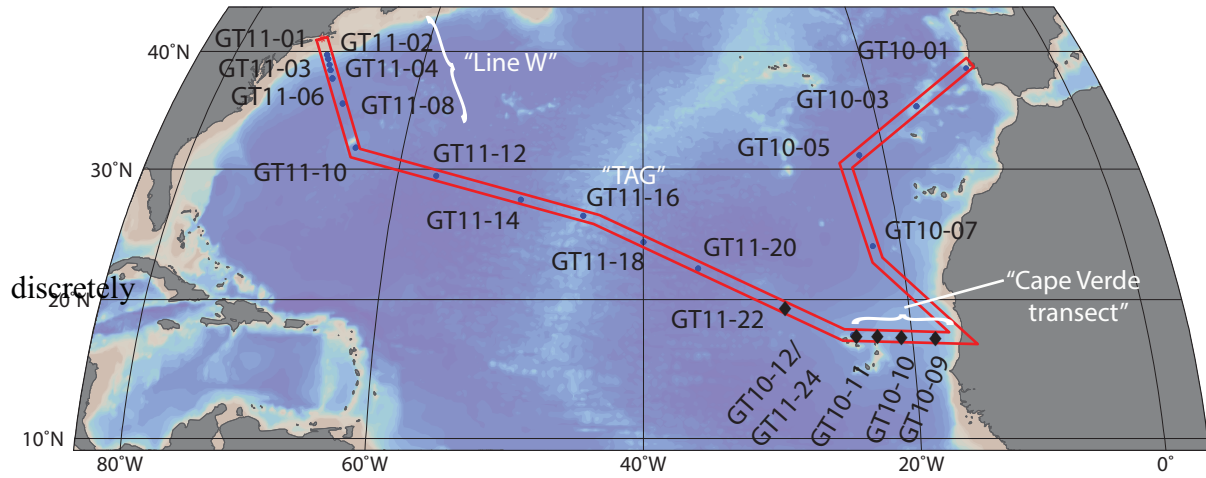
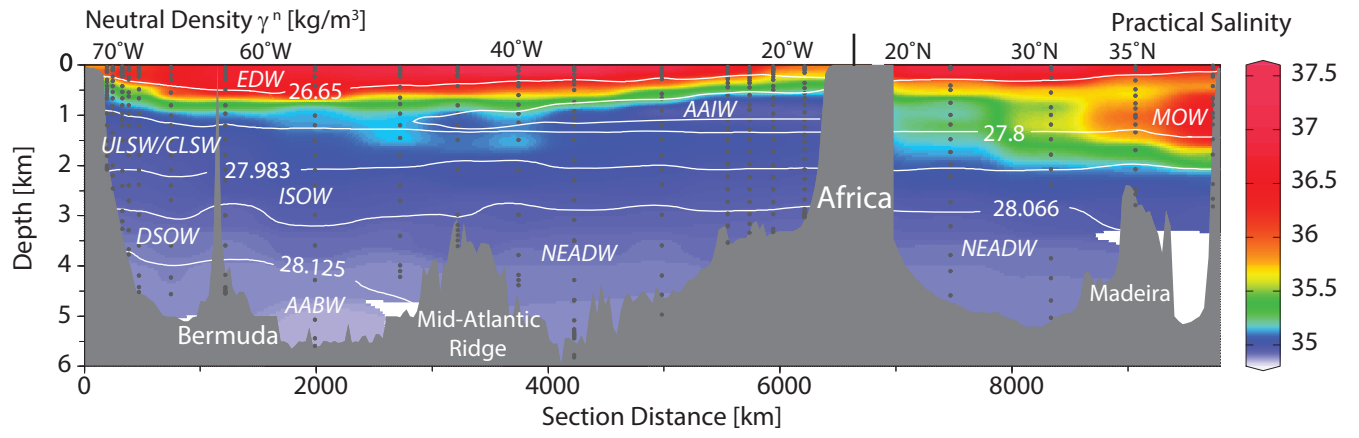
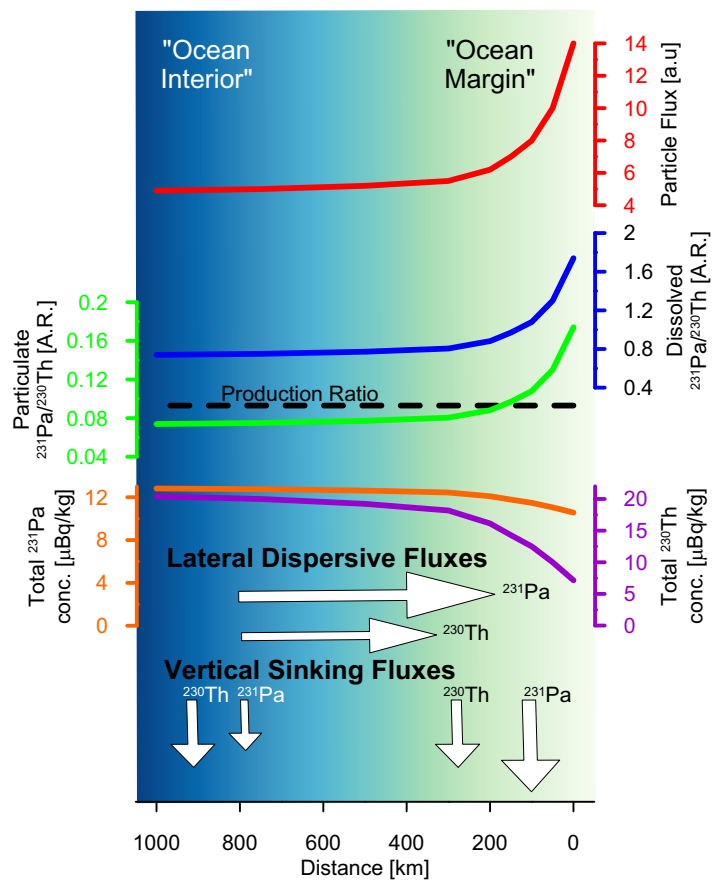


Figure 1



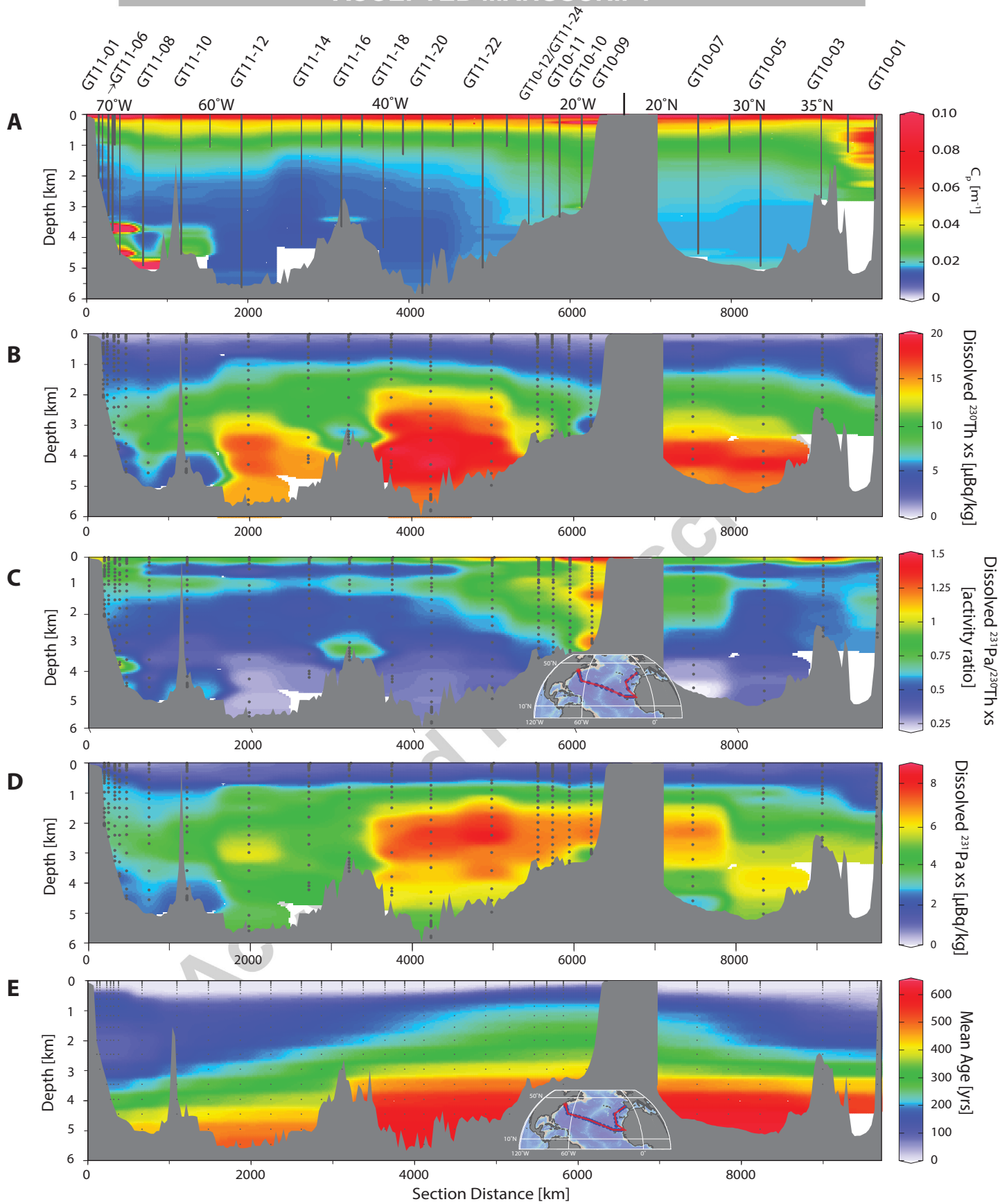
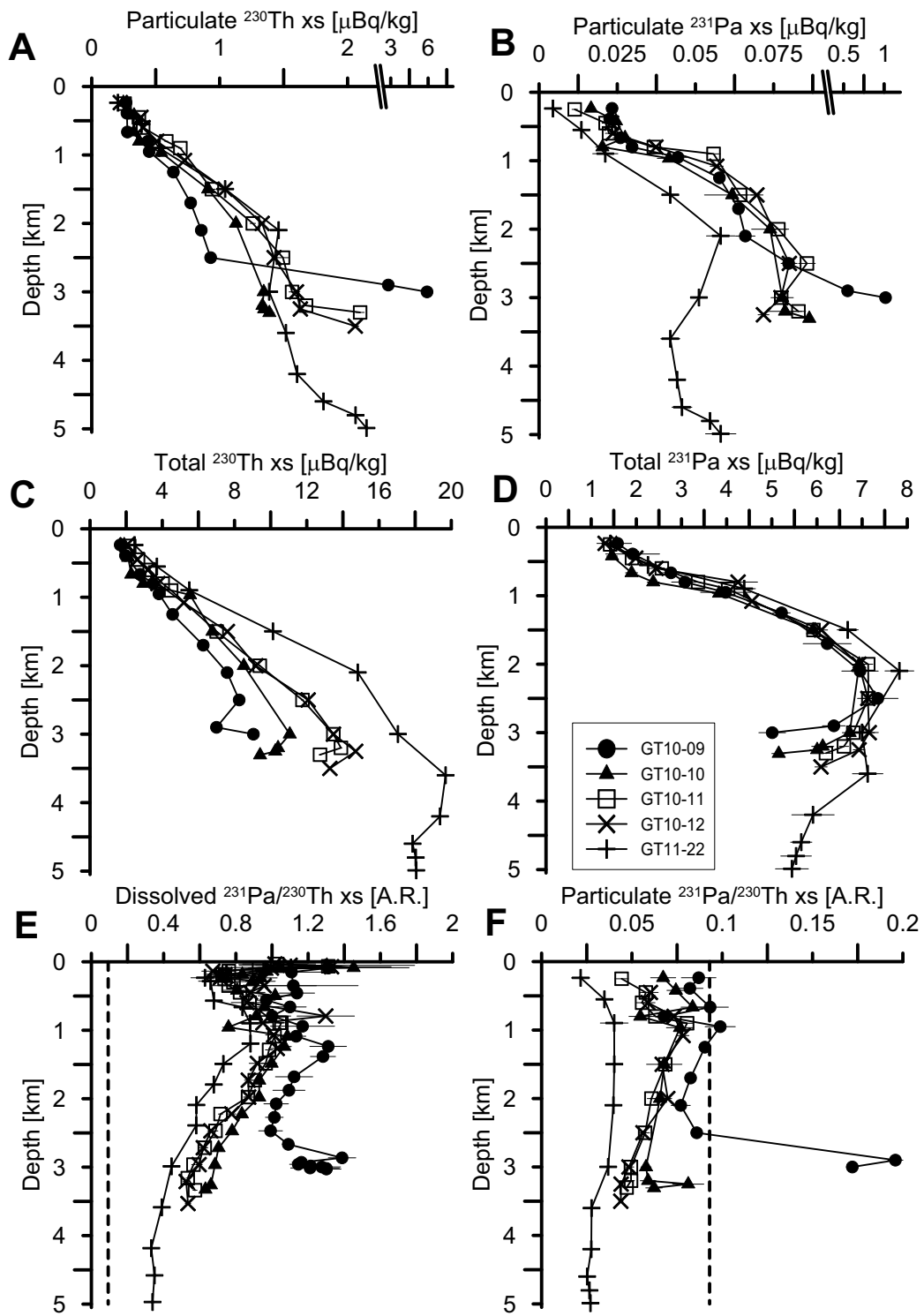
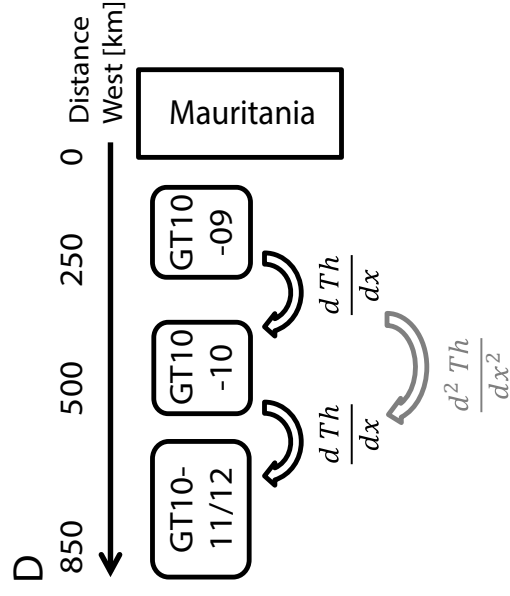
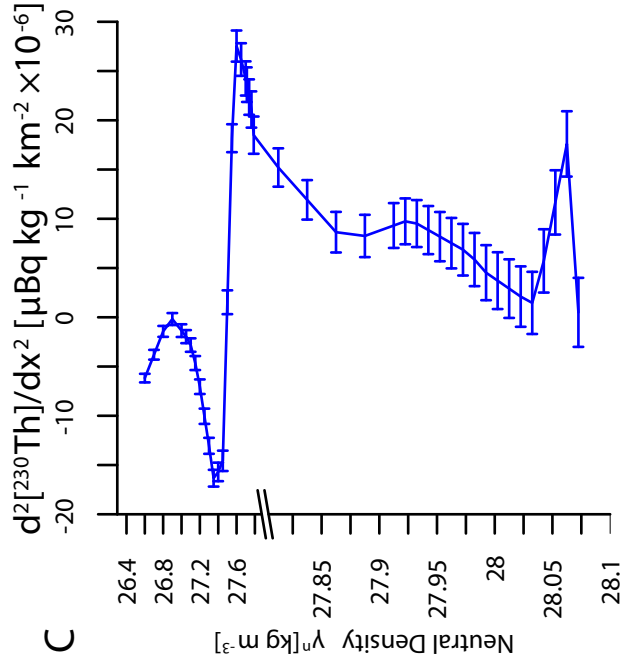
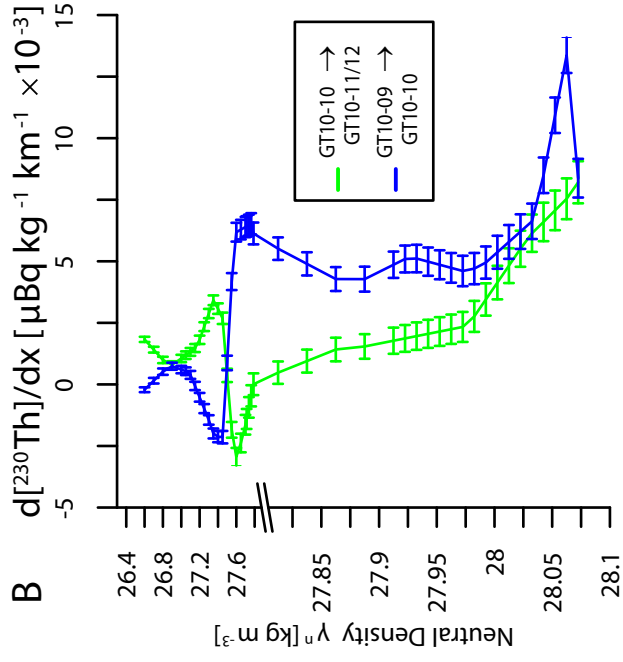
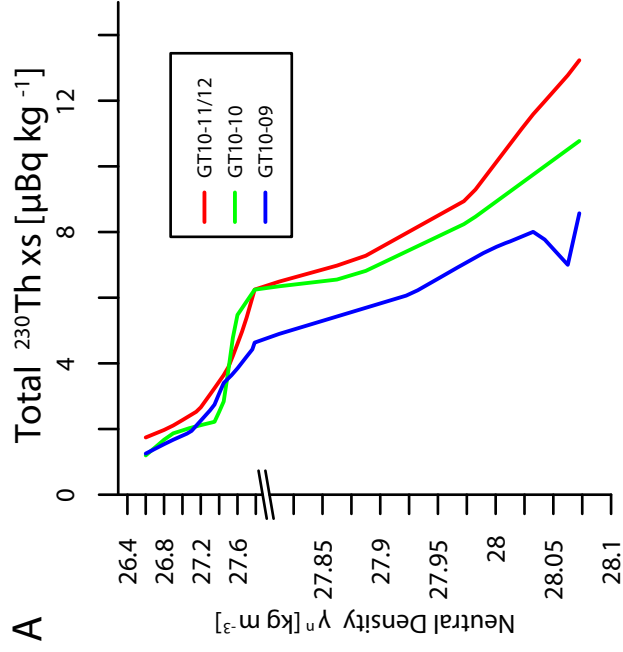
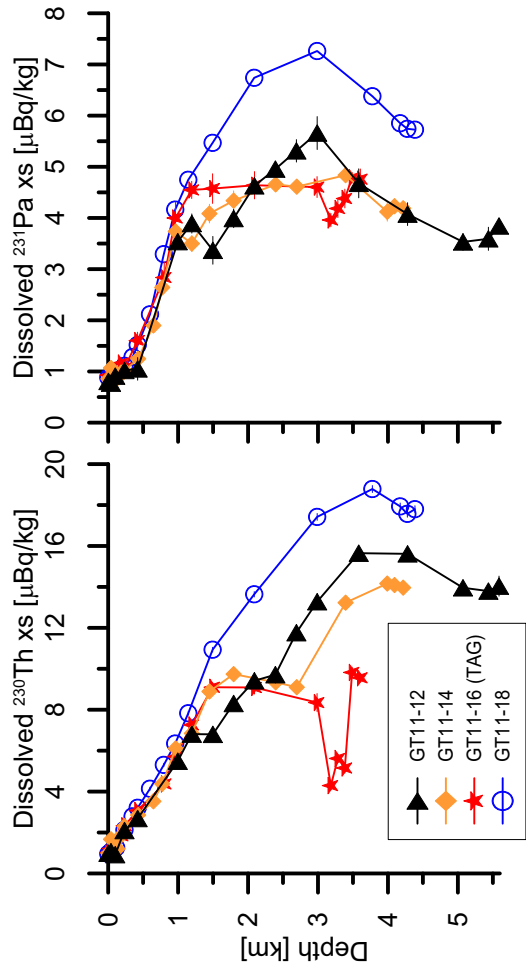


Figure 3.







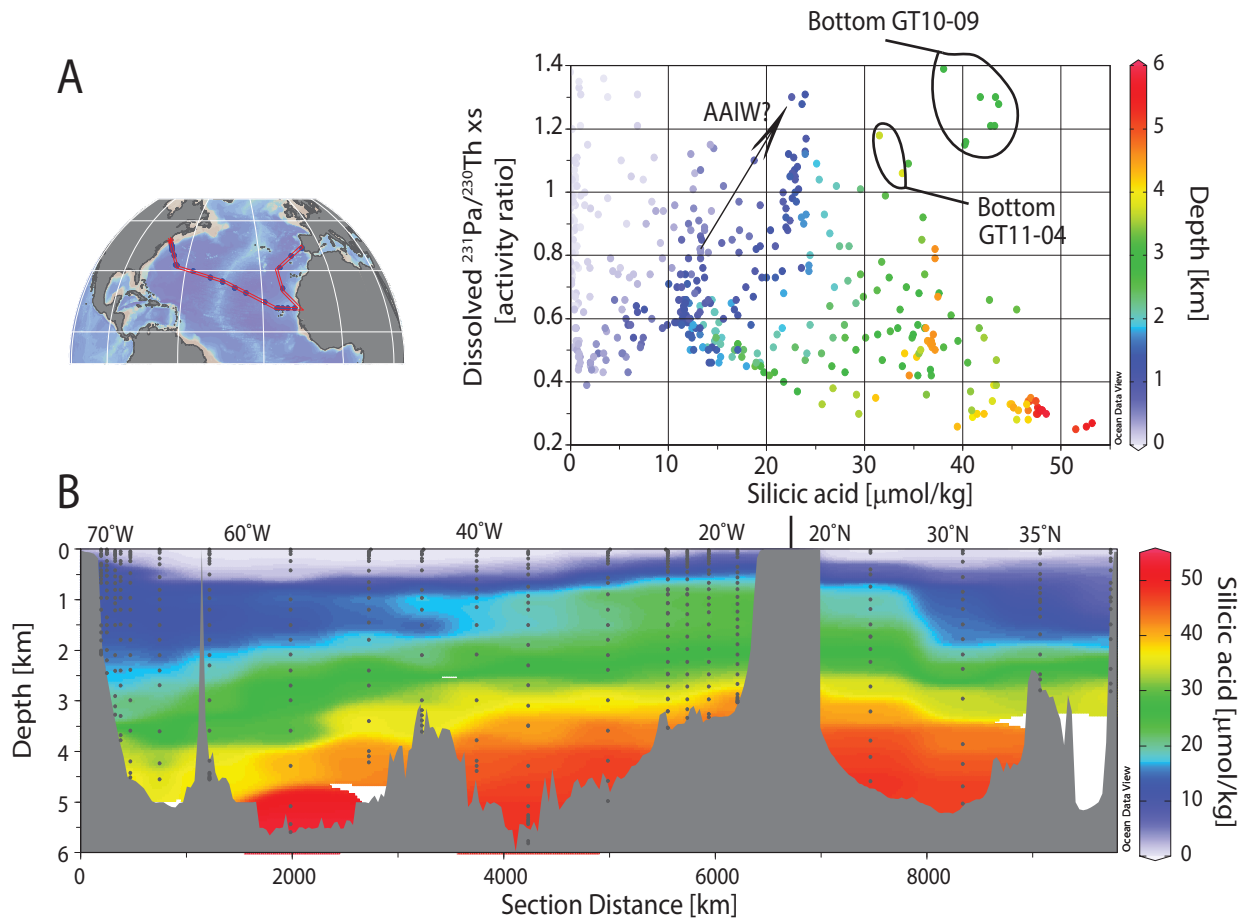


Figure 7.